

ATHENA: Agentic Team for Hierarchical Evolutionary Numerical Algorithms

Juan Diego Toscano^a, Daniel T. Chen^a, George Em Karniadakis^{a,1}

^a*Division of Applied Mathematics, Brown University, Providence, 02912, RI, USA*

Abstract

Bridging the gap between theoretical conceptualization and computational implementation presents a significant bottleneck in Scientific Computing (SciC) and Scientific Machine Learning (SciML). Here, we introduce ATHENA (Agentic Team for Hierarchical Evolutionary Numerical Algorithms), an agentic framework designed as an Autonomous Lab to manage the complete end-to-end computational research lifecycle. Its core is the HENA loop, a knowledge-driven diagnostic process designed as a Contextual Bandit problem. In this framing, the system acts as an online learner: at each step, it analyzes the history of prior trials and observables to select a structural ‘action’ (A_n) from a combinatorial space guided by expert-derived blueprints (e.g., Universal Approximation, Physics-Informed constraints). This action is translated into executable code (S_n) to generate a composite scientific reward (R_n), driving a no-regret policy. We demonstrate that this structured reasoning allows ATHENA to transcend standard automation: in SciC, it autonomously identifies deep mathematical symmetries to discover exact analytical solutions or identifies physical properties of the problem to obtain stable and accurate numerical solvers where foundation models fail. In SciML, it moves beyond hyperparameter tuning to perform deep physical diagnosis, autonomously detecting and developing methods to tackle ill-posed formulations or combining hybrid symbolic-numeric workflows (e.g., coupling PINNs with FEM for AI Velocimetry) to resolve complex multiphysics problems. The framework achieves super-human performance, reaching validation errors of the order of 10^{-14} for canonical benchmarks. Furthermore, we show that ATHENA operates as a symbiotic partner; in “human-in-the-loop” regimes, collaborative intervention allows the system to bridge the “Valley of Death” in stability, improving results by an order of magnitude. This paradigm shifts the researcher’s focus from implementation mechanics to methodological innovation, significantly accelerating algorithmic and scientific discoveries.

Keywords: physics-informed learning, PINNs, neural operators, adaptive sampling, PDEs

1. Introduction

The rapid ascent of Foundation Models (FMs) [1, 2] has fundamentally altered the landscape of scientific research, offering unprecedented capabilities in data synthesis, code generation, and hypothesis formation [3]. In the domain of Applied Mathematics and Scientific

¹Corresponding author: george.karniadakis@brown.edu

Computing, these models hold the promise of automating the development of rigorous Numerical Methods [4], the essential mathematical algorithms required to solve the Partial Differential Equations (PDEs) that govern physical reality [5, 6]. From high-order spectral schemes [7] to Physics-Informed Neural Networks (PINNs) [8] for inverse problems, these methods serve as the ‘engine’ of computational discovery, demanding not merely syntactic correctness but strict adherence to mathematical guarantees of stability, consistency, and convergence. However, bridging the gap between the probabilistic text generation of modern AI and the deterministic rigor required for high-fidelity numerical simulation remains a profound challenge[9].

Despite the transformative capabilities of foundation models, their deployment as autonomous researchers is fundamentally constrained by three intrinsic cognitive bottlenecks that limit the scope of single-agent workflows. First, as the complexity of a scientific problem grows, the reliance on massive context windows triggers the “Lost in the Middle” phenomenon [10], where models fail to retrieve or adhere to constraints buried within extensive technical documentation. Second, the autoregressive nature of text generation makes long-horizon reasoning susceptible to “conceptual drift” [11]; without intermediate correction, minor logical errors accumulate exponentially [12], causing the final implementation to diverge from the initial scientific intent. Finally, these models suffer from a lack of perception, operating as “blind” generators that cannot visually inspect their own output, such as loss curves or solution fields, to verify physical consistency [13]. These limitations necessitate a shift away from monolithic models toward multi-agent systems capable of distributing these cognitive loads. Therefore, several researchers have explored and developed agentic frameworks to accelerate scientific discovery, with significant progress on three major fronts: high-level conceptualization, specialized numerical automation, and advanced evolutionary search.

In the domain of high-level reasoning, pioneering work has focused on the “idea generation” phase. The “SciAgents” framework, for instance, introduces a powerful multi-agent system that navigates a large-scale ontological knowledge graph to discover and critique novel, interdisciplinary research hypotheses, outputting a full research proposal [14]. Complementing this, “Flexible Swarm Learning” presents a compelling conceptual argument for moving away from monolithic models, proposing a decentralized “swarm learning” architecture of small, adaptive agents as a more efficient way to model complex, dynamic systems [15]. While these frameworks are powerful “planners”, they are not designed as “executors,” stopping short of the fully autonomous implementation and iterative validation of their conceptual proposals.

A second category of research has tackled the bottleneck of practical implementation by building “specialist tools” to automate specific difficult tasks. In the PINN domain, “PINNSAgent” tackles hyperparameter optimization (HPO) by using a vast 3,000-experiment database to inform a “Memory Tree Reasoning” search for optimal configurations [16], while “Lang-PINN” offers a multi-agent system that translates a natural language description into a complete executable PINN workflow [17]. Beyond PINNs, other tools aim to simplify complex workflows, which leads to lowering the technical barrier to complex ODE parameter estimation by automatically translating a user’s Python code into a high-performance, JAX-based pipeline [18]. Similarly, “MetaChat” accelerates nanophotonic design by linking a natural language interface to a pre-trained millisecond-fast surrogate solver [19]. While

these powerful “specialist tools” excel at their defined tasks, their focus is on optimization rather than autonomous scientific reasoning, as they are not designed to diagnose scientific failures and prescribe structural architectural cures.

A third and highly advanced category of evolutionary search-based frameworks has emerged. This philosophy has been powerfully demonstrated by systems that optimize code for “scorable” tasks with a fast evaluation loop. For example, the “AlphaEvolve” agent, which discovers novel solutions to pure mathematics problems, can explore “deep trees” by sampling thousands of potential solutions [20]. Similarly, the framework by Aygün et al. relies on this search strategy to discover expert-level empirical software [21]. However, this approach is computationally intractable for complex SciML problems, where a single experiment can take hours to run.

Building on these principles, the “AgenticSciML” framework is the first to apply a similar evolutionary philosophy directly to complex SciML tasks [22]. The authors propose a collaborative system of over 10 agents that can debate, propose, and refine solutions to bridge both conceptualization and numerical execution, achieving order-of-magnitude improvements. However, to overcome the computational intractability of a “brute-force” search, its “ensemble-guided evolutionary search” is heavily constrained, exploring a much shallower tree of only 15-20 total solutions for a given problem. Furthermore, this search is guided by a “data-driven method memory”.

In parallel to this data-driven and search-based work, an alternative knowledge-driven paradigm is emerging. This knowledge-first philosophy is evident in related fields, such as the autonomous engineering design framework by [23], which employs specialized knowledge-graph-building agents to guide its reasoning. Moreover, across these emerging frameworks, whether search-based or knowledge-driven—the architectural design of the multi-agent collaboration often appears heuristic and structurally arbitrary. Current systems typically lack a formal mathematical objective governing agent interactions. Without such a framework to structure the hierarchy, it is difficult to design a framework that systematically improves over time rather than drifting into instability or redundancy.

To address this structural gap, we draw inspiration from the theory of Online Learning. In practice, scientific research is generally not a monolithic process, but rather an iterative cycle of high-level strategy and practical execution. We interpret this lifecycle not as a trajectory through a hidden state space, but as a Contextual Bandit problem (see [24, Chapter 18] for an introduction). Under the random outcome of stochastic solvers and generative processes, the researcher must use predefined strategies, formed based on prior knowledge and outcomes of past experiments, to navigate an uncertain environment. Formally, at each step n , the system observes the history of prior trials to select a research plan or action A_n from a finite action space. This action is converted into an executable code state S_n , which is executed to produce observations O_n . These results are analyzed to qualify the results (i.e., reward R_n).

To operationalize this theoretical framework, we introduce the HENA (Hierarchical Evolutionary Numerical Algorithms) loop. In this architecture, specific Agentic Teams are explicitly assigned to manage each stage of the bandit formulation. The Implementation Teams function as the ‘execution operator,’ responsible for translating the abstract research plan into the concrete code state S_n and generating the observations O_n . Conversely, the Conceptualization Teams function as the ‘policy,’ responsible for analyzing the history of these observations to formulate the next structural action A_n and assign the reward R_n .

To impose structure on the otherwise intractable combinatorial search space, we construct our policy around an organizing principle we call “Conceptual Scaffolding”. Rather than attempting to feed the model thousands of raw papers, which would trigger the “Lost in the Middle” phenomenon, we constrain the action space using a minimalist set of expert-derived blueprints that provide core mathematical constraints (e.g., approximation theorems [25, 26, 27, 28], optimization principles [29], etc.). This mathematically grounded search space aims to induce a submartingale on the scientific reward (i.e., $\mathbb{E}[R_{n+1}|\text{History}_n] \geq R_n$), i.e., the search process aims to be more efficient than random guessing.

This scaffolding-based policy is not a fixed lookup table of solutions; it is a generative reasoning process. It grants the agents a “constrained freedom” to innovate within established scientific principles. In practice, this is executed by our Advisor agents. Within the HENA loop, these agents use the scaffolding’s fundamental knowledge to diagnose scientific failures and reason about the most logical structural evolution. This diagnostic process addresses the model’s inherent lack of perception, enabling the system to visually verify its own outputs and transcend standard automation. Specifically, it allows the model to devise methods to recover exact solutions, apply physical constraints to obtain stable numerical solvers, and improve the state-of-the-art results on both human and agentic benchmarks in PIML, with errors as low as 10^{-14} .

By exploiting this efficiency, we have constructed a complete general-purpose “Agentic SciML Lab,” named ATHENA (Agentic Team for Hierarchical Evolutionary Numerical Algorithms). This framework applies HENA across three separate task domains: Scientific Computing, PINNs, and Operator Learning. Beyond simple automation, ATHENA orchestrates complex hybrid workflows, such as coupling data-driven SciML models with rigorous classical solvers (SciSolver) to resolve multiphysics problems. While it operates in a fully autonomous mode for standard benchmarks, it is specifically designed as a transparent partner for “expert-in-the-loop” regimes. We demonstrate that this collaborative intervention allows a human researcher to guide high-level decisions and improve final performance by an order of magnitude, effectively shifting the human’s role from low-level debugging to high-level conceptualization.

2. Methods

2.1. Online Learning as a Model for Agentic Research

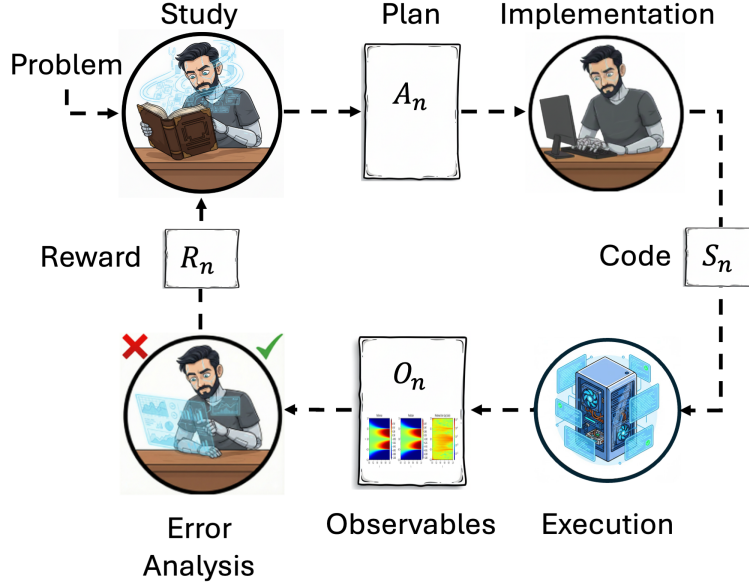


Figure 1: **Online Learning as a Model for Agentic Research.** This diagram illustrates the research lifecycle modeled as a Contextual Bandit problem. The cycle begins with the Study phase (Policy π), where the Strategist synthesizes the Problem context and prior Rewards (R_n) to formulate a structural Plan or Action (A_n). The Implementation phase (Operator \mathcal{I}) translates this abstract plan into executable Code or State (S_n). Following Execution, the raw Observables (O_n)—such as loss curves and solution fields—are processed by the Error Analysis (Advisor) agent. Crucially, this agent computes the Scientific Reward (R_n), closing the feedback loop and enabling the system to iteratively minimize regret in subsequent trials.

In practice, scientific research is not a monolithic process, but rather an iterative cycle of high-level strategy and practical execution (See Figure 1). We interpret this lifecycle not as a trajectory through a hidden state space, but as a Contextual Bandit problem (see [24, Chapter 18] for an introduction). Under the random outcome of stochastic solvers and generative processes, the researcher must use predefined strategies—formed based on prior knowledge and outcomes of past experiments—to navigate an uncertain environment.

Formally, at each step n , the system observes the history of prior trials and selects a research plan or action A_n from a finite action space \mathcal{A} . This action is converted into an executable code state S_n , which is executed to produce observations O_n . These results are analyzed to assign a scalar reward R_n .

The above process is repeated based on a predetermined policy, a collection

$$\pi = (\pi(A_n | A_1, O_1, R_1, \dots, A_{n-1}, O_{n-1}, R_{n-1}))_{n \in \mathbb{N}}$$

of stochastic kernels, that determines the next action A_n based on previous actions, observations, and rewards. The quality of such a policy is quantified using regret, defined as the difference in rewards between the actions taken and the (in retrospect) optimal action. For

a time horizon $T > 0$, the regret is defined to be

$$\text{Regret}_T(\pi) = \mathbb{E}_\pi \left[\sum_{t=1}^T R^* - R_t \right]$$

where R^* is the expected reward from playing the optimal action. Non-trivial policies are those that achieve a vanishing regret, i.e., $\text{Regret}_T(\pi)/T \rightarrow 0$ as $T \rightarrow \infty$.

Note that we omit the state variable S_n from the high-level bandit formalization. We regard the code state variations as statistical fluctuations rather than a major conceptual piece of the generative process.

Our objective is not to *learn* this policy from scratch, but to *design* a specific fixed policy that is demonstrably sample-efficient. This policy encapsulates human-level diagnostic expertise to induce a probabilistic bias toward higher-reward states. More specifically, we aim for this expert-designed process to induce a submartingale on the expected reward:

$$\mathbb{E}[R_{n+1} \mid \text{History}_n] \geq R_n.$$

This formalizes the intent of our design: *to create an intelligent search process that is strictly more efficient than random guesses.*

2.2. HENA: Hierarchical Evolutionary Numerical Algorithms

To operationalize the online learning framework, we introduce HENA (Hierarchical Evolutionary Numerical Algorithms). HENA is organized into two primary logical groups: the Conceptualization Teams (Strategy and Advisor), which function as the high-level policy π , and the Implementation Teams (Collection, Implementation, and Debugging), which function as the execution operator \mathcal{I} . Both groups are composed of multiple specialized LLM-based agents.

We formalize the iterative agentic loop as follows. For the n -th iteration, the transitions read:

$$\begin{aligned} A_{n+1} &\sim \pi(A_{n+1} \mid A_1, O_1, \dots, A_n, O_n) && \text{(policy update)} \\ S_n &\sim \mathcal{I}(S_{n-1}, A_n) && \text{(implementation)} \\ O_n &\sim E(O_n \mid S_n) && \text{(observation)} \end{aligned}$$

Here, $A_n \in \mathcal{A}$ is the structural action (research plan) derived from the history. The operator \mathcal{I} (Equation [implementation](#)) is the implementation function. It must translate the abstract action A_n into a concrete executable code state S_n . This task requires complex reasoning; therefore, we instantiate \mathcal{I} using a team of coding agents that engage in an iterative refactoring loop. Crucially, this subprocess involves an Inspector Agent that strictly verifies that the code follows the proposed strategy. Because this guarantees that S_n is a faithful realization of the requested blueprint A_n regardless of prior history, the resulting code state satisfies the Markov property required for the bandit formulation ($S_n \perp S_{n-1} \mid A_n$).

To strictly adhere to the Contextual Bandit formulation defined in the previous section, the system is designed to satisfy three additional theoretical constraints. First, the actions A_n must be drawn from a finite combinatorial action space \mathcal{A} . We define \mathcal{A} as a combinatorial

space derived from a modular decomposition of the problem. For instance, in Physics-Informed Machine Learning (PIML), following previous work, we decompose the problem into modular subspaces:

$$\mathcal{A} = \mathcal{A}_{rep} \times \mathcal{A}_{constraint} \times \mathcal{A}_{opt}.$$

In this example, \mathcal{A}_{rep} represents the representation model (e.g., MLP, KAN, Polynomials), $\mathcal{A}_{constraint}$ denotes the physics enforcement strategy (e.g., strong form, weak form), and \mathcal{A}_{opt} defines the optimization strategy. This ensures that the action space covers the necessary search volume while remaining discrete and learnable. Second, the policy must balance exploiting known effective methods with exploring uncertain potential solutions. We enforce this by carefully designing the system prompts of the Conceptualization Teams, explicitly encouraging the agents to explore new methods (exploration) even after obtaining valid solutions to avoid premature convergence.

Third, to enforce the no-regret property, we must define a reward function $R(A_n, O_n)$ that is attainable. In scientific computing, a residual of absolute zero is often impossible due to floating-point arithmetic. Therefore, to ensure that the optimal strategy yields a maximum reward, allowing regret to converge to zero, we construct a composite reward function based on four independent evaluation axes:

$$R_n = R_{integrity} + R_{accuracy} + R_{details} + R_{optimality}.$$

The first component, integrity ($R_{integrity}$, 35 pts), measures the executability and interpretability of the code state. The second component, accuracy ($R_{accuracy}$, 35 pts), evaluates quantitative success and is further decomposed into precision (S_{prec}), which assesses if error falls below a dimensional threshold (e.g., $\epsilon \approx 10^{-3}$), and consistency (S_{cons}), which evaluates adherence to constraints. The third component, details ($R_{details}$, 15 pts), functions as a qualitative penalty term for local failures (e.g., Gibbs oscillations). Finally, the optimality component ($R_{optimality}$, 15 pts) rewards computational efficiency. By capping the requirements for perfect accuracy at physically meaningful thresholds rather than mathematical zero, we ensure that the optimal policy is attainable, thereby satisfying the condition for vanishing regret.

2.3. Conceptual Scaffolding: Constraining the Policy Search

Conceptual Scaffolding is our practical implementation of the fixed sample-efficient policy, π_{HENA} , required by the Contextual Bandit formulation. As defined in the previous sections, the agent must select an action A_n from a combinatorial space \mathcal{A} to minimize regret. However, without constraints, \mathcal{A} is effectively infinite, making the no-regret objective computationally intractable. Furthermore, standard LLMs are prone to proposing hallucinated solutions that lie outside the valid mathematical solution manifold.

Our scaffolding addresses these theoretical challenges by acting as a prior that constrains the action space. This design also addresses a critical practical limitation: the finite context window of Large Language Models. While arguably one could feed thousands of papers directly into the prompt to provide knowledge, active research indicates that LLM performance tends to deteriorate as the context size grows—a phenomenon often referred to as being “Lost in the Middle”. By distilling this vast literature into compact blueprints, our framework circumvents this degradation. This constraint is imposed via two primary

mechanisms: system prompts and base code templates. Importantly, these blueprints do not prescribe specific rigid combinations; rather, they define fundamental constraints that allow for generative flexibility. For instance, under the Universal Approximation blueprint, the model is free to employ any univariate function for a KAN architecture, provided it serves as a valid universal approximator. The system prompts explicitly encode this modular decomposition, forcing the agents to reason within specific structural boundaries rather than generating free-form text. Simultaneously, the base templates provide valid executable starting points for every action category, ensuring that the agents modify existing robust structures rather than writing code from scratch. These two mechanisms effectively prune the search tree, ensuring that every proposed action $A_n \in \mathcal{A}$ is mathematically grounded.

The scaffolding content is organized into five initial blueprints (detailed in the Appendix), each targeting a critical domain of the research lifecycle. These include the Universal Approximation Blueprint (guiding architectural choices), the Physics-Informed Machine Learning Blueprint (handling PDE constraints), the Operator Learning Blueprint (managing function-to-function mappings), the Optimization Blueprint (navigating non-convex landscapes), and the Numerical Methods Blueprint (for classical method selection). We do not claim that these blueprints summarize the entirety of these vast fields; rather, they serve as a starting point to ground the agents.

This structured guidance is what empowers the meta-reasoning operator π , instantiated by the Advisor and Strategy Teams. Instead of randomly sampling the full action space, the agents use the scaffolding to perform a knowledge-driven local search in the policy space. This allows them to map the observed failures O_n (e.g., high-error regions in a plot) to a specific principled cure A_{n+1} (e.g., "apply adaptive sampling") derived from the blueprints. This grounding is what enables the policy to be generative—discovering novel solutions like a Wavelet-KAN—while remaining robust, modular, and aiming to induce the submartingale property $\mathbb{E}[R_{n+1}] \geq R_n$ on the expected reward.

2.4. ATHENA (*Agentic Team for Hierarchical Evolutionary Numerical Algorithms*)

Our complete agentic framework, ATHENA (Agentic Team for Hierarchical Evolutionary Numerical Algorithms), is illustrated in Figure 2. The architecture is organized into four distinct logical groups (A-D). The process begins with the Conceptualization Group (Figure 2 A, Red), which acts as the user-facing triage system. The User interacts with a Coordinator to formalize a problem, and the Gatekeeper routes this User Request to the appropriate generative group or the Storage Group, effectively establishing the formal problem definition.

This initialization triggers the core HENA (Hierarchical Evolutionary Numerical Algorithms) loop—comprising Groups B, C, and D—which operationalizes the Contextual Bandit formulation described in the previous section. This loop is driven by the ‘policy’ operator (π) teams (Figure 2 B, Green), which represent the “brain” of the system. This group, containing the Strategy and Advisor Teams, receives the full history from previous cycles and formulates the new high-level structural action, A_n . To address the known limitation of LLMs regarding the lack of intrinsic verification and awareness of consequences, this group employs a proposer-critic architecture where a Critic Agent validates the Strategist’s plan. This plan A_n is then passed to the ‘implementation’ operator (\mathcal{I}) teams (Figure 2 C, Blue).

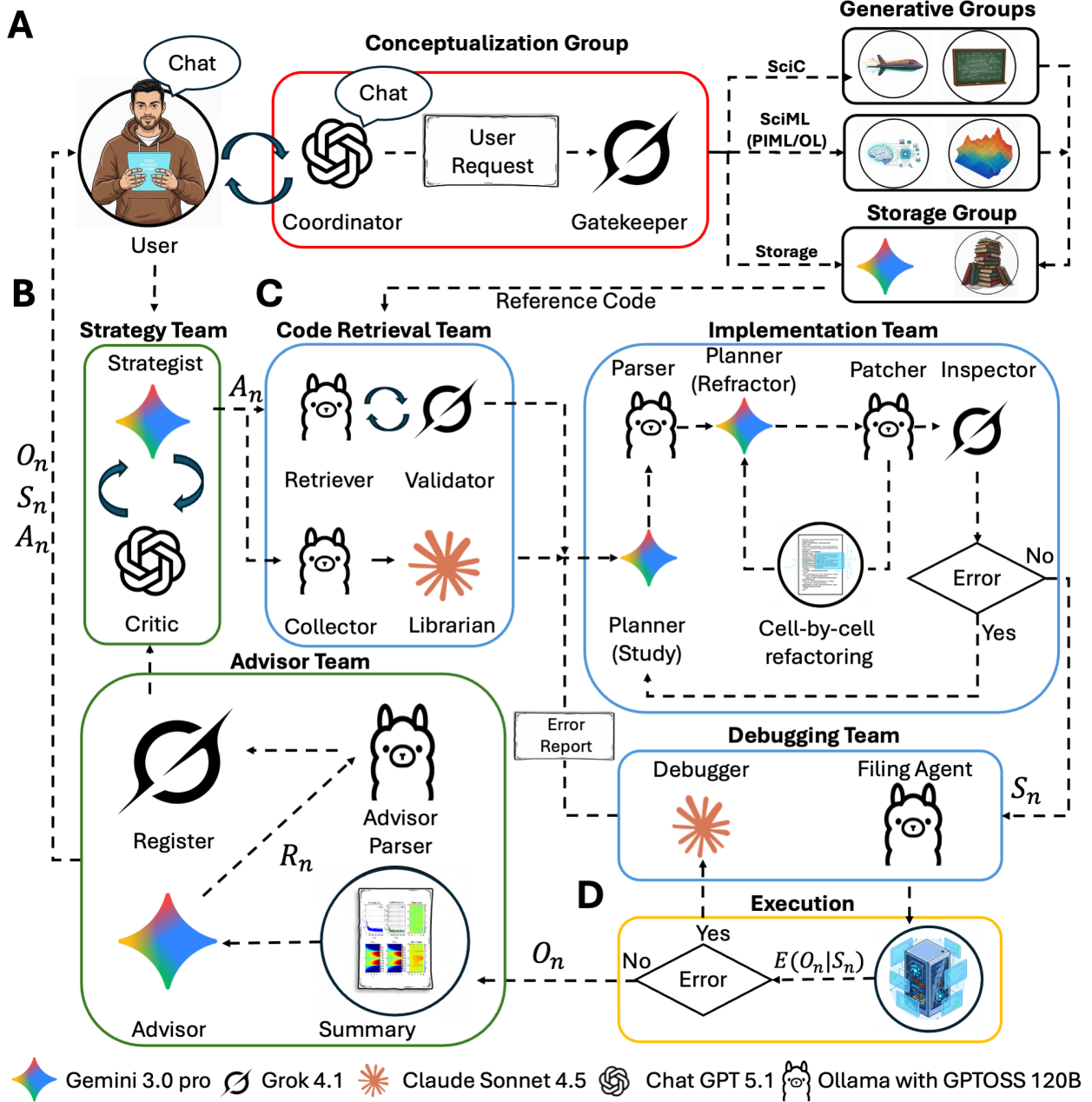


Figure 2: **ATHENA (Agentic Team for Hierarchical Evolutionary Numerical Algorithms)**. The framework is organized into four logical groups, with specific icons indicating the heterogeneous allocation of Large Language Models (LLMs) to specialized roles (see legend). (A) The Conceptualization Group (Red): The user-facing triage system. The User interacts with a Coordinator to define a User Request, which the Gatekeeper routes to the appropriate team. (B) The ‘Policy’ Operator π (Green): The “brain” of the HENA loop, composed of the Strategy Team and Advisor Team. This group analyzes the context C_n to formulate the structural action A_n and assigns the scientific reward R_n based on the resulting observations. (C) The ‘Implementation’ Operator \mathcal{I} (Blue): The “executor” teams (Code Retrieval, Implementation, Debugging) that build, patch (“cell-by-cell refactoring”), and debug the code to produce the executable state S_n . Crucially, this workflow includes an Inspector Agent, which strictly verifies that the implementation faithfully follows the desired plan A_n before execution. (D) The Execution Block (Yellow): This component runs the observation function $E(O_n|S_n)$ on the state S_n to generate the multi-modal observation O_n (plots, logs). This observation O_n is sent back to the Advisor Team (B), completing the evolutionary cycle. The user also has access to A_n , S_n , and O_n at each iteration, enabling a transparent expert-in-the-loop workflow.

The execution phase begins with the Code Retrieval Team. To prevent the downstream Planner agent from succumbing to the “Lost in the Middle” phenomenon caused by excessive context, this team functions as an intelligent filter. It employs an Agentic RAG system to retrieve the most suitable base templates and, crucially, performs Agentic RAG Generation to autonomously synthesize missing modules (e.g., custom layers) that are guaranteed to be compatible with the retrieved context. This ensures the Planner receives a focused cohesive codebase, significantly simplifying its reasoning task.

Once the context is prepared, the Implementation Team handles the assembly. This group is designed to mitigate the *autoregressive error accumulation*—formally known as conceptual drift—inherent in long-context generation. Since the probability of a correct sequence decays exponentially with length ($P(\text{correct}) \approx p^N \rightarrow 0$), monolithic generation is mathematically prone to divergence. To mitigate this, the group employs a strict ‘cell-by-cell refactoring’ protocol driven by a Planner Agent. This agent operates in two focusing stages: first, it studies the codebase to identify only the specific cells requiring modification; second, it targets the refactoring exclusively to those cells. This containment strategy enables the framework to robustly generate and maintain extensive scientific codebases scaling to thousands of lines of code. To further address the lack of consequence awareness at the code level, the workflow includes an Inspector Agent. This agent acts as a verifier, strictly auditing the Planner’s modifications against the desired plan A_n before the code produces the final executable state, S_n . If runtime errors occur, the Debugging Team is activated to iteratively patch the code until execution is successful.

Finally, the state S_n is processed by the Execution block (Figure 2 D, Yellow), which runs the observation function $E(O_n|S_n)$ on the state S_n to generate the multi-modal observation, O_n (e.g., plots and logs). This observation O_n is sent back to the Advisor Team (Green), which analyzes it to generate the scientific reward R_n and the diagnostic report, completing the cycle. Importantly, the key components of each cycle (A_n , S_n , O_n) are available to both the agent teams and the user, creating a transparent, fully closed-loop system. Furthermore, the final validated codes from successful experiments are fed back to the Storage Group, allowing the framework’s knowledge base to grow over time. A detailed description of each agent’s role is provided in Appendix B. The framework is designed to be model-agnostic, currently supporting leading foundation models such as GPT-5.1 [30], Gemini 3.0 [31], Claude 4.5 [32], and Grok 4.1 [33](See Figure 2).

3. Results

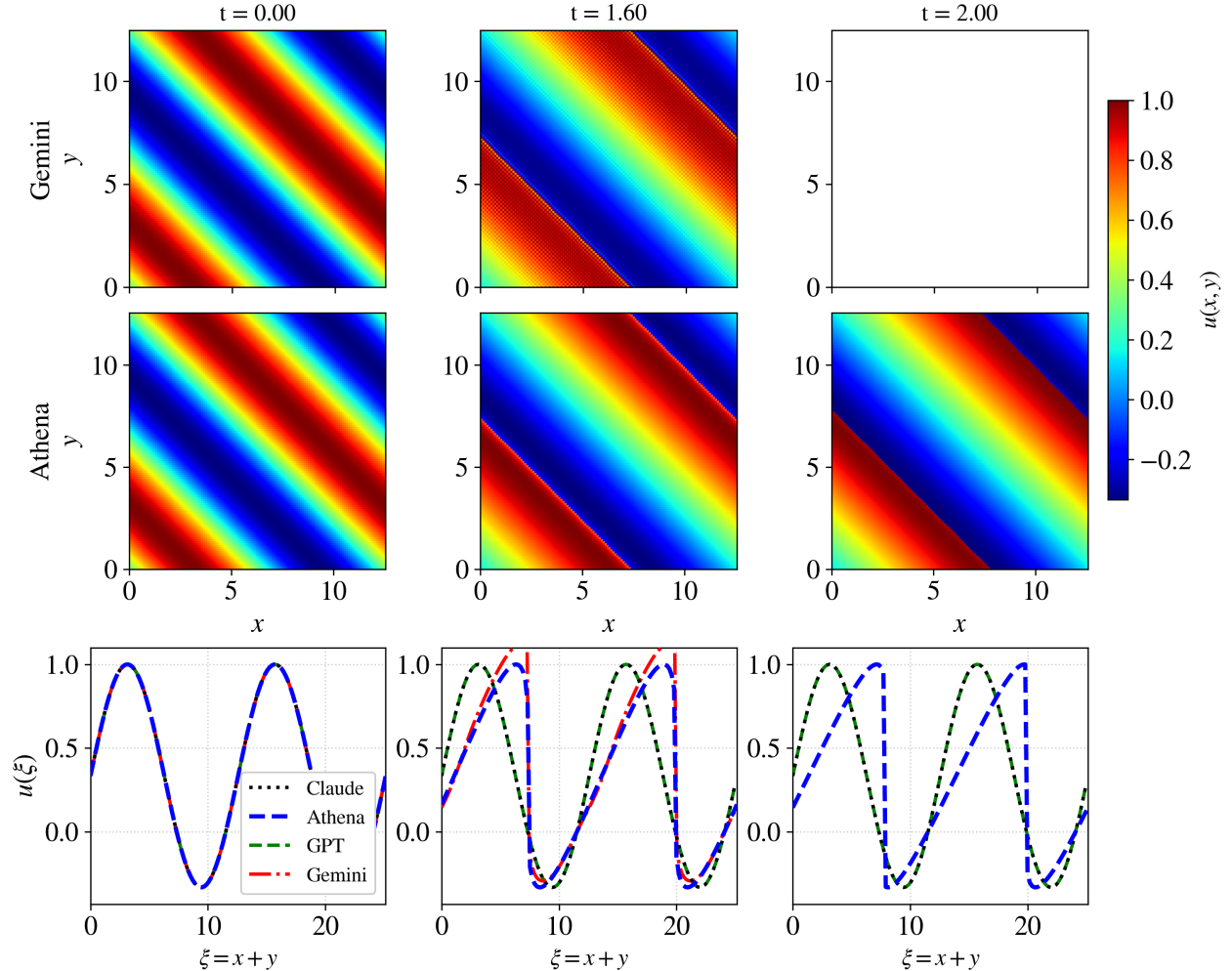


Figure 3: **Comparative analysis of the 2D Inviscid Burgers’ benchmark.** The panels contrast the solution fields generated by state-of-the-art foundation models via direct prompting against the autonomous solution discovered by ATHENA. Baselines (Direct Prompting): Models such as GPT-5.1 and Claude Sonnet 4.5 incorrectly select Fourier Spectral methods and apply aggressive frequency filtering to handle the shock, resulting in “arrested motion” where the wave fails to propagate. Gemini 3.0 captures the dynamics but succumbs to significant instability and oscillations at the shock interface. ATHENA (Ours): By leveraging its agentic scaffolding, ATHENA diagnoses the problem’s underlying symmetry and autonomously switches to the Method of Characteristics. This allows it to bypass numerical diffusion entirely and recover the Exact Solution (ground truth), validating the framework’s ability to transcend naive numerical selection.

3.1. ATHENA identifies the best method to solve the problem

ATHENA demonstrates the capability to identify and deploy the optimal computational strategy by first utilizing its Data Collection Team—the Receptionist and Gatekeeper agents—to extract problem specifications and constraints. Based on this intake, the system acts beyond a simple selector; it autonomously configures highly specialized solvers: for classical numerical tasks, it deploys high-order methods like Spectral Fourier [34] or Discontinuous Galerkin [35, 36] with necessary stability controls (e.g., adaptive mesh refinement [37],

limiters, shock indicators [38, 39], etc.), while for data-driven problems, it bypasses generic baselines in favor of expert-driven initializations, such as optimal feature embeddings and KANs for PINNs or orthogonal decompositions for Operator Learning. Crucially, our results show that ATHENA is not limited to a binary choice between paradigms; it successfully proposes and orchestrates hybrid workflows, such as leveraging classical solvers to generate high-fidelity synthetic data for training SciML models, or conversely, utilizing SciML for rapid inverse approximations that are subsequently refined by rigorous numerical methods to ensure final accuracy.

3.2. ATHENA uncover hidden exact solutions when available

To demonstrate the framework’s capacity for deep physical reasoning, we analyze the 2D Inviscid Burgers’ equation (Figure 3), a benchmark where traditional numerical schemes, such as Finite Difference or Finite Volume [40], inevitably introduce discretization errors and diffusion that obscure the ground truth. While finding an exact analytical solution for arbitrary 2D initial conditions is typically considered intractable, ATHENA transcended standard numerical paradigms by identifying deep mathematical symmetries. The Strategist Team analyzed the specific initial conditions and velocity field, instructing the system to:

Rewrite the PDE in quasi-linear form $u_t + u u_x + u u_y = 0$ and view this as advection with velocity field $\mathbf{a}(u) = (u, u)$. By defining the Lagrangian coordinate $s_0 = x_0 + y_0$, the mapping from the initial state to the current state s is given implicitly by $s = s_0 + 2u_0(s_0)t$.

This insight permitted the use of the Method of Characteristics to derive an exact implicit solution, completely bypassing the errors inherent in numerical PDE solvers. Moreover, during the implementation phase, the framework exhibited physics-informed reasoning to resolve operational failures. When the code execution failed with a convergence error—caused by the instability of the Secant method as the solution steepened into a shock—the Planner Agent avoided random hyperparameter tuning. Instead, it analyzed the underlying physics to derive a strict bound:

The previous error report indicates a convergence failure; we must switch to a robust bracketing method. The displacement $|s_{\text{target}} - s_0|$ is strictly bounded by $2 \cdot \max|u_0| \cdot t$, which yields a maximum displacement of 4. Therefore, a search interval of ± 5 is safe.

This derivation allowed the agent to define a "safe" search interval based on the maximum wave speed, switching to a robust bracketing method that guaranteed convergence where standard algorithms failed. The necessity of this agentic scaffolding is highlighted by the comparative analysis in Figure 3. When prompted directly, state-of-the-art models (GPT-5.1, Claude Sonnet 4.5, Gemini 3.0) failed to solve the problem, defaulting to Fourier Spectral methods that struggled with the shock discontinuity. Specifically, GPT-5.1 and Claude 4.5 aggressively filtered high frequencies to mitigate oscillations, causing the wave motion to arrest completely, while Gemini 3.0 succumbed to instability at the shock interface. Crucially, ATHENA utilizes these very same models as sub-agents; yet, by constraining them within our framework, it prevents these naive numerical failures and instead guides them to uncover the exact analytical solution.

3.3. ATHENA finds conceptual errors and refines solutions

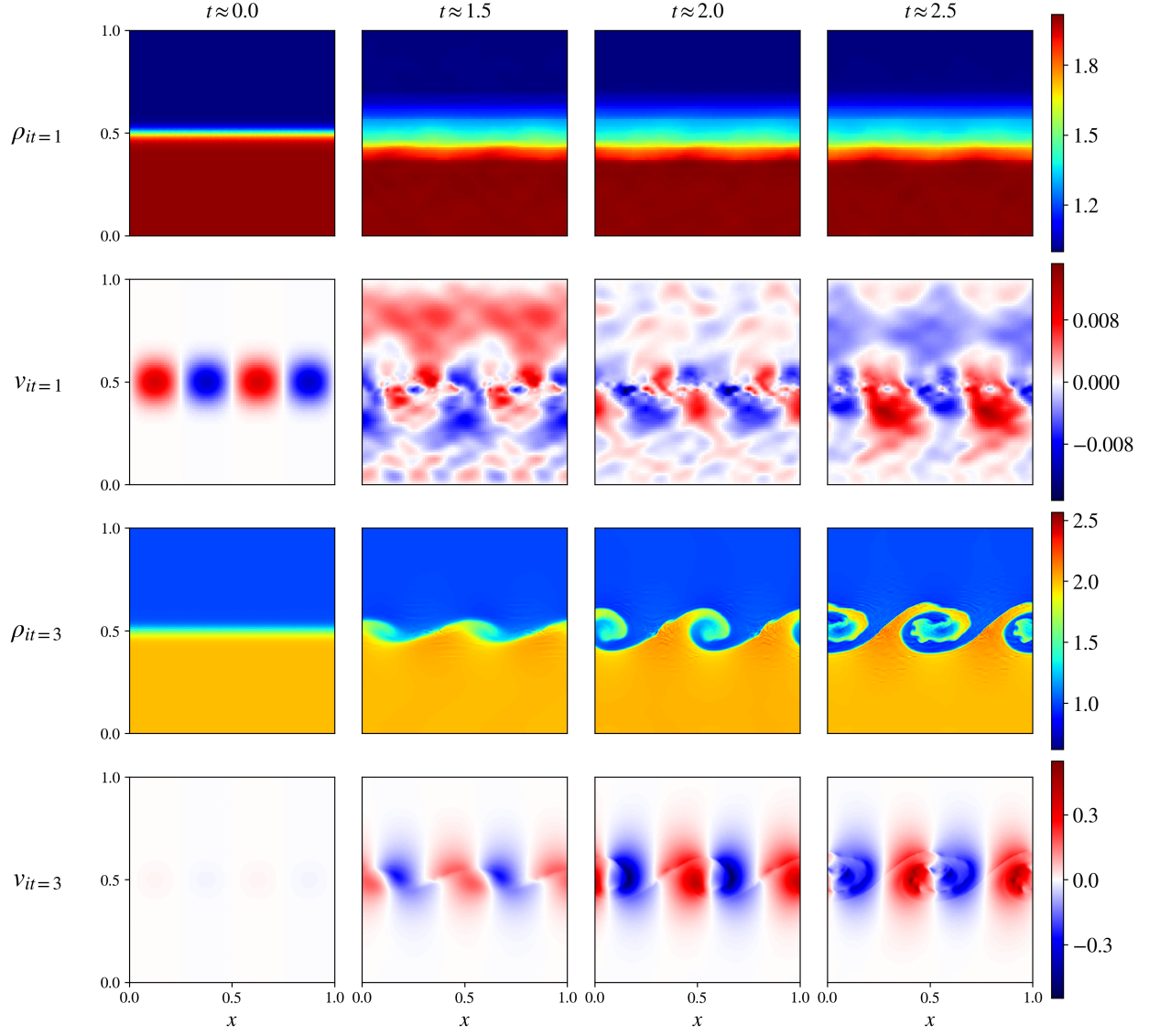


Figure 4: **Autonomous correction of the Kelvin-Helmholtz Instability (Euler Equations)** The figure tracks the evolution of the solution fields—Density (ρ) and Velocity (v)—as ATHENA refines the solver configuration. Rows 1-2 (Iteration 1): The initial simulation completes with exit code 0 but exhibits a “silent physics failure.” The solution is dominated by numerical diffusion; the shear layer is smeared, and the vortices fail to form because the velocity-based AMR indicator cannot distinguish the interface. Rows 3-4 (Iteration 3): Following the Advisor Team’s intervention—which switched the AMR trigger to density, increased the polynomial order, and tuned shock capturing—the system recovers the correct inviscid dynamics. Note the emergence of sharp, well-defined Kelvin-Helmholtz rolls and the characteristic “cat’s eye” vortex structures, demonstrating the restoration of physical fidelity.

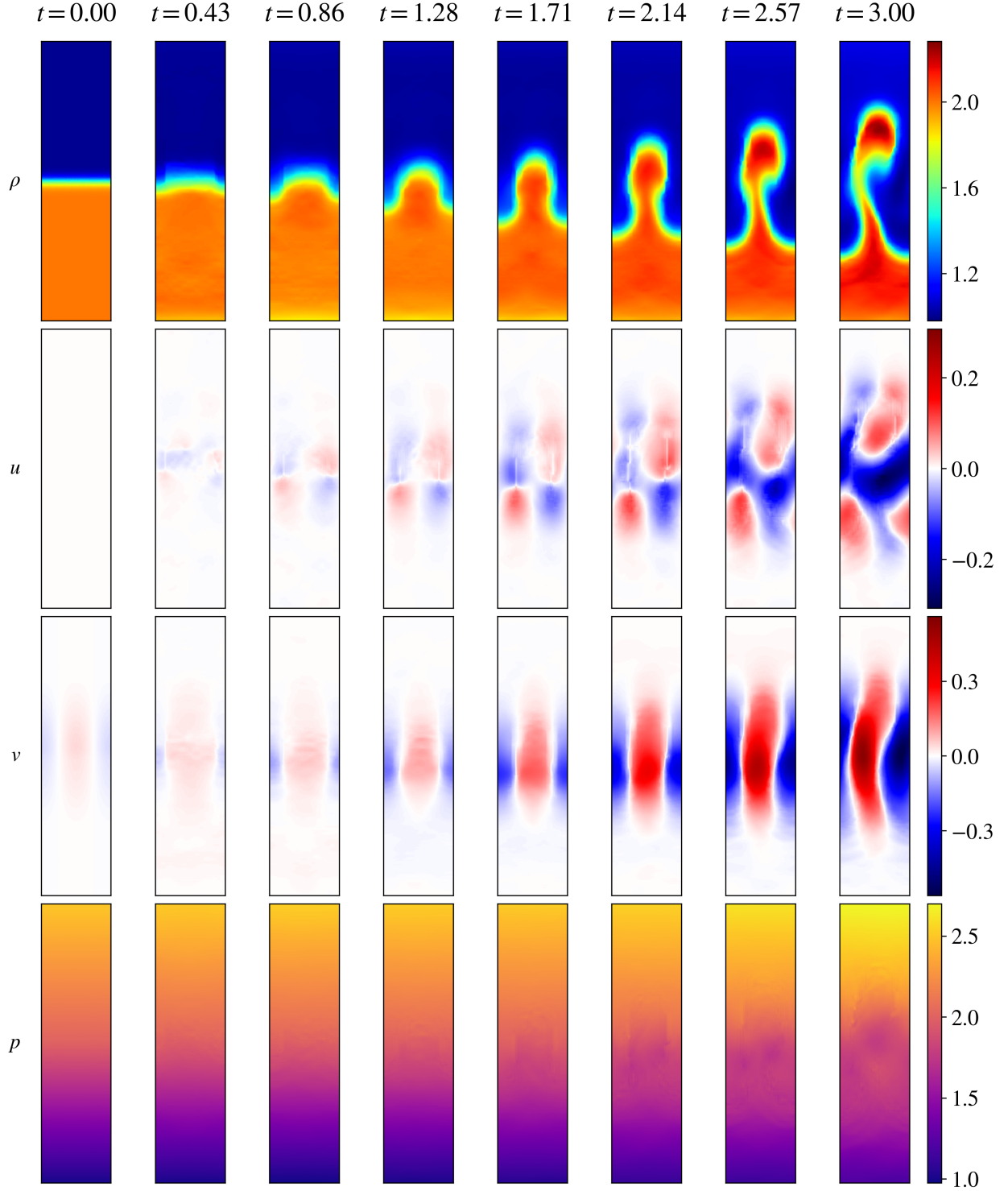


Figure 5: **Rayleigh-Taylor Instability (Compressible Navier-Stokes).** Time evolution of density (ρ), velocity (u, v), and pressure (p). Unlike baselines that failed due to geometric distortions or instability, ATHENA stabilized the simulation by autonomously diagnosing two critical constraints: (1) It reconfigured the mesh topology into a 1×4 quadtree forest to match the domain's 1:4 aspect ratio, preventing element stretching. (2) It analytically derived and enforced the exact hydrostatic pressure gradient ($\nabla p = \rho \mathbf{g}$) to balance the piecewise density. These interventions prevented spurious acoustic waves, allowing the complex non-linear mixing to develop stably.

To challenge the framework’s capabilities beyond simple benchmarks, we tasked ATHENA with simulating two canonical instabilities governed by non-linear conservation laws: the Kelvin-Helmholtz instability, modeled by the hyperbolic Euler equations (see Figure 4), and the Rayleigh-Taylor instability, governed by the compressible Navier-Stokes equations (see Figure 5). These problems are notoriously difficult due to their extreme sensitivity to numerical dissipation and geometric constraints, serving as a definitive stress test for the framework’s ability to orchestrate rigorous scientific code.

In the Kelvin-Helmholtz case, a critical distinction emerged in how the framework handled the initial execution. While the first iteration completed successfully with an exit code of 0, the results were dominated by numerical diffusion, effectively solving viscous equations rather than the intended inviscid dynamics. Instead of blindly tuning hyperparameters, the Advisor Team analyzed the smeared results and diagnosed the issue as a physical disconnect between the mesh sensors and the flow features. The agent provided a precise structural correction:

Major Physics Failure: The Kelvin-Helmholtz instability failed to develop, and the solution exhibits excessive smearing. The current AMR indicator uses ‘velocity magnitude,’ which is symmetric and low-contrast at the shear layer center. Switch the AMR indicator to Density (ρ) or Vorticity, which have distinct peaks at the interface. Furthermore, increase polydeg from 3 to 5 to reduce dispersion error, and loosen the shock indicator threshold, as it is currently activating on the contact discontinuity and killing the inviscid instability physics.

This intervention forced the solver to switch to density-based refinement, allowing it to resolve the delicate shear instability that naive configurations smoothed out.

Similarly, the Rayleigh-Taylor instability required the agents to navigate complex geometric and physical initialization constraints. The user specified a tall domain with a 1:4 aspect ratio, which typically leads to severe element stretching and degradation of accuracy when using standard square templates. The Planner Agent autonomously recognized this topological mismatch and reconfigured the mesh connectivity, stating:

Physical domain $\Omega = [0, 0.25] \times [0, 1.0]$ `trees_per_dimension=(1, 4)` constructs the root connectivity as a 1x4 arrangement of quadtrees to match the domain’s aspect ratio.

Furthermore, to prevent spurious acoustic waves from crashing the simulation, the agent analytically enforced the required hydrostatic balance. It integrated the governing equations for the specific piecewise density profile to derive the exact pressure gradient, ensuring a stable physical start:

Pressure... is initialized in hydrostatic equilibrium, where the pressure gradient balances the gravitational force... implemented as a piecewise linear function. ...

$$p = 2.0 * y_coord + 1.0 \text{ if } y < 0.5 \text{ else } y + 1.5.$$

The success of these simulations highlights the robustness of the resulting code. In both cases, ATHENA successfully deployed a Discontinuous Galerkin Spectral Element Method (DGSEM) written in Julia[41, 42, 43] with several state-of-the-art methods such as adaptive

mesh refinement, shock indicators, and others. This represents a significant leap in complexity compared to standard code generation; notably, when we presented these same problem specifications to state-of-the-art models (GPT-5.1, Claude Sonnet 4.5, and Gemini 3.0), none were able to produce runnable code for these batches. By combining deep physical reasoning with high-order numerical methods, ATHENA constructs valid, stable, and highly accurate solvers where direct prompting fails.

3.4. ATHENA achieves highly accurate results on canonical PIML problems

In our initial evaluation across a suite of canonical benchmarks—ranging from the Allen-Cahn and viscous Burgers equations to the Helmholtz and KdV systems—ATHENA consistently achieves better performance than human experts and established agentic benchmarks. As detailed in Table 1, the framework demonstrates remarkable precision, achieving mean squared errors as low as 10^{-14} and a minimum relative L^2 error of 5.34×10^{-9} for the viscous Burgers equation, orders of magnitude superior to the baselines. Beyond raw metrics, the agents demonstrated profound methodological versatility: they autonomously adapted to varying initial conditions for the Allen-Cahn equation (Figure 6(a)), implemented the Method of Manufactured Solutions to verify steady-state Helmholtz solvers (Figure 7 (a)), and performed symbolic manipulation to extract and enforce differentiable boundary conditions for the KdV system (Figure 7 (b)), all without human intervention.

This performance is driven by the Strategist Agent’s adherence to the “Conceptual Scaffolding,” which treats the PINN as a modular assembly of specialized components [44], that is specifically input transformations [45, 46], representation model modifications [47, 48, 49, 50], and Output transformations [51, 52, 53, 54]. Contrary to monolithic black-box approaches, this modularity enables targeted improvements to the architecture without needing to rewrite the solver. For instance, the Strategist knows that minimizing the L-infinity norm is preferable but not stable, so it must employ dual formulations like Variational Residual-Based Attention (vRBA) [29] so it uses adaptive weights [55, 56, 57, 58, 59] or sampling [60, 61, 62, 63, 64], often paired with aggressive second-order such as SSBroyden [65, 66, 67, 68]. This structural awareness was demonstrated when a user required periodic boundary conditions; rather than adding a soft loss term, the agent mandated a precise architectural modification:

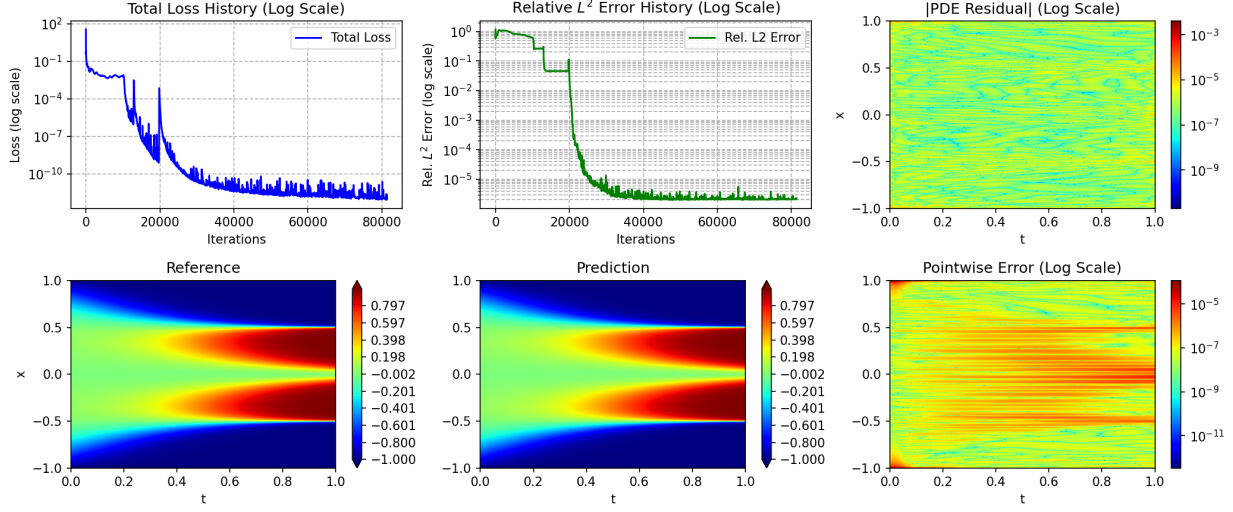
To enforce this constraint directly and efficiently, the Planner must modify the model architecture... to incorporate the Periodic Fourier Features layer. This is a critical requirement. ... the embedding_degree for the periodic features must be set to a very low value, specifically degree=1.

By treating the architecture as the constraint, the agent proactively prevented numerical instability. Crucially, the visualizations presented in Figures 6 and 7 are not merely post-hoc evaluations but the actual observations utilized by the Advisor Agent at the end of each stage. The Advisor has access to these specific plots, showing prediction manifolds, pointwise residuals, and loss histories, to diagnose the solver’s state. This visual feedback allows it to catch nuances that automated metrics miss. In one instance, despite achieving a low error of 10^{-7} , the Advisor rejected the result based on a visual inspection of the loss history:

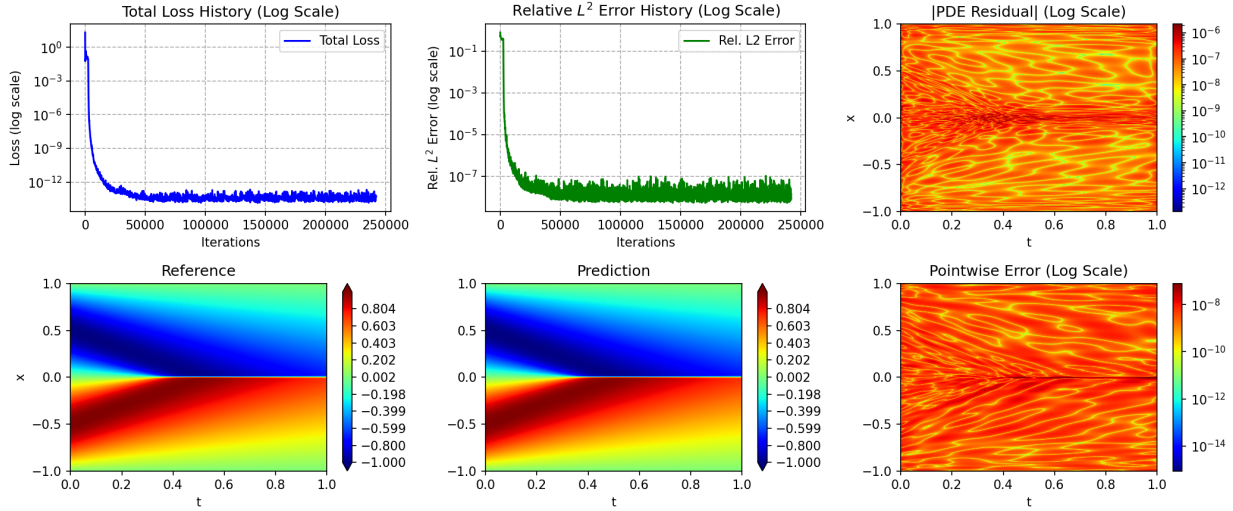
A visual inspection of the last half of the ‘Relative L2 Error History’ plot... clearly shows that the error is still actively decreasing and has not yet plateaued. This

*indicates that the model has not fully converged to its minimum achievable error...
Recommend duplicating the number of iterations...*

This insight, derived directly from the observed figures, forced the system to continue training until true convergence was reached, distinguishing between a merely good approximation and a scientifically optimal result.



(a) Allen-Cahn

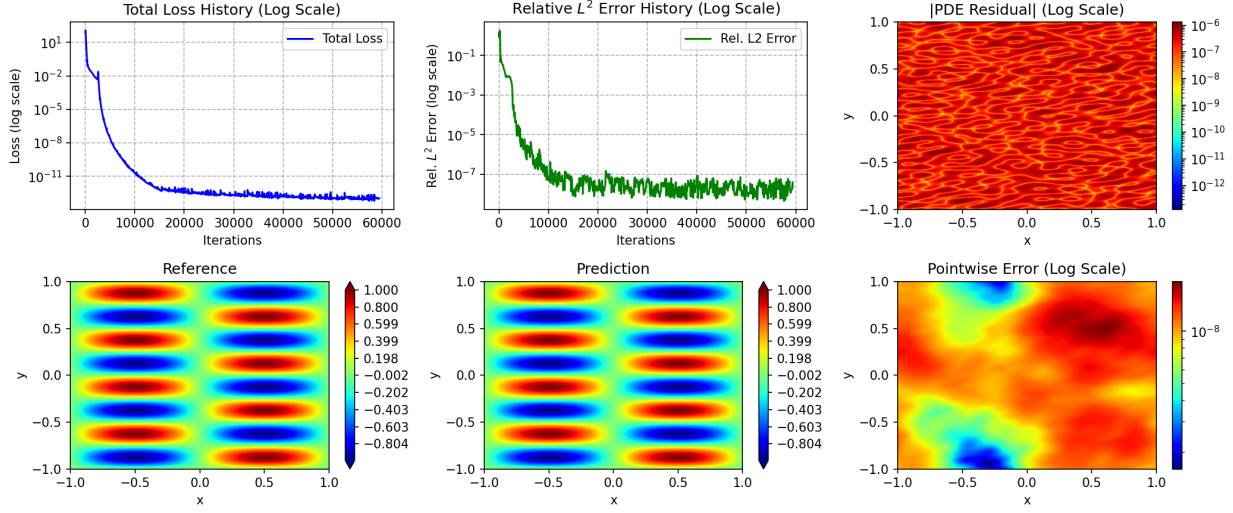


(b) Viscous Burgers

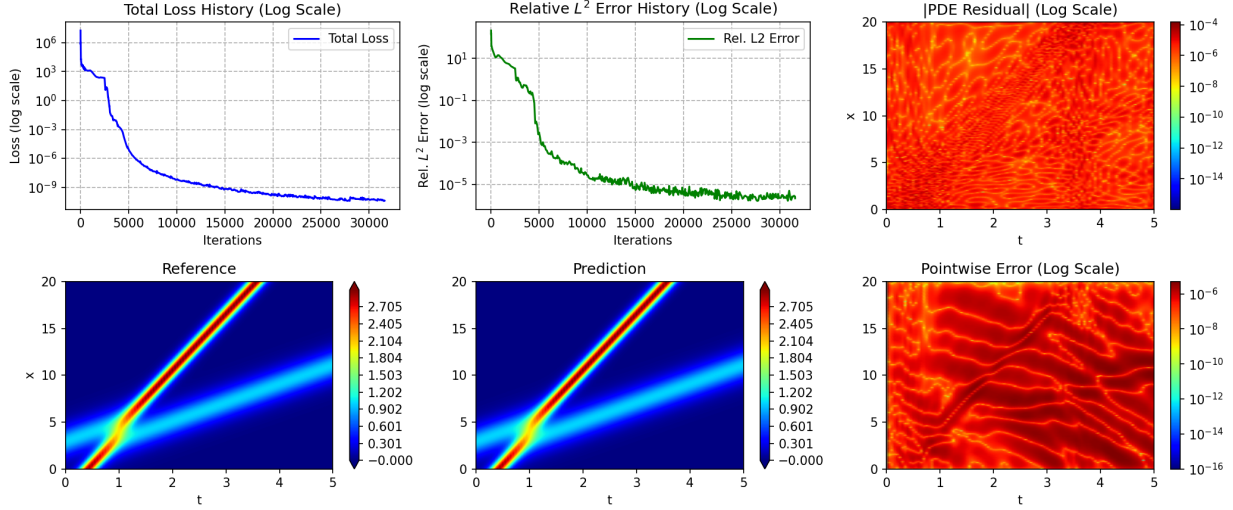
Figure 6: Diagnostic dashboards for canonical benchmarks. These panels represent the exact visual state observed by the Advisor Agent at the end of the training stage. **(a) Allen-Cahn:** The system successfully captures the sharp phase transitions from the cosine initialization. **(b) Viscous Burgers:** The system resolves the shock formation with high fidelity ($MSE \sim 10^{-14}$). For both cases, the first row displays the loss and error histories used to verify convergence stability. The second row presents the reference solution, the ATHENA prediction, and the pointwise error. The bottom row visualizes the pointwise PDE residual map. Note that in (b), the residuals appear distinctively intense due to the Strategist's choice to employ Variational Residual-Based Attention (vRBA) with an exponential potential, forcing an aggressive L_∞ minimization.

Table 1: **Quantitative comparison against state-of-the-art baselines.** We evaluate ATHENA across five canonical benchmarks, contrasting performance with recent expert-authored publications (Human) and emerging agentic frameworks. Dominance in Accuracy: ATHENA consistently achieves lower error rates, notably reaching an MSE of 4.76×10^{-14} for the Viscous Burgers equation—surpassing competing agents by nine orders of magnitude. Human-Level Parity: For the Helmholtz and KdV systems, the framework autonomously delivers solutions that exceed the accuracy of manually tuned baselines.

Problem	Reference	Benchmark Type	Rel. L^2 Error	MSE
Allen Cahn	[69]	Human	3.48×10^{-6}	—
	[65]	Human	2.20×10^{-6}	—
	[70]	Human	1.45×10^{-5}	—
	[29]	Human	2.14×10^{-6}	—
	(Ours)	Agents	1.94×10^{-6}	6.31×10^{-13}
Burgers ($\nu = \frac{1}{100\pi}$)	[69]	Human	4.03×10^{-5}	—
	[70]	Human	1.38×10^{-4}	—
	[16]	Agents	—	6.51×10^{-5}
	[17]	Agents	—	6.48×10^{-5}
	[65]	Human	2.90×10^{-6}	—
	[66]	Human	1.62×10^{-8}	—
	[29]	Human	1.51×10^{-8}	—
	(Ours)	Agents	5.34×10^{-9}	4.76×10^{-14}
Helmholtz	[65]	Human	3.60×10^{-7}	—
	[70]	Human	4.86×10^{-5}	—
	(Ours)	Agents	2.22×10^{-8}	1.01×10^{-13}
KdV	[65]	Human	6.00×10^{-6}	—
	(Ours)	Agents	2.21×10^{-6}	4.10×10^{-11}
Inviscid Burgers	[71]	Human	1.20×10^{-1}	—
	[72]	Human	8.30×10^{-2}	—
	(Ours)	Agents	1.35×10^{-3}	3.78×10^{-7}
	(Ours)	Agents + Human	3.23×10^{-4}	2.64×10^{-7}



(a) Helmholtz (Method of Manufactured Solutions)



(b) Korteweg-de Vries (KdV)

Figure 7: Verification of advanced methodological capabilities. These dashboards illustrate how the Advisor Agent validates complex problem setups beyond standard data fitting. **(a) Helmholtz:** Demonstrates the successful application of the Method of Manufactured Solutions (MMS). The agent verifies the steady-state solver by comparing it against a fabricated source term, ensuring the implementation correctly balances the Laplacian and the wavenumber k . **(b) KdV:** Showcases the system’s symbolic reasoning. The Strategist Agent autonomously extracted the analytical solution, implemented it in a differentiable format, and rigorously enforced the extracted Dirichlet and Neumann boundary conditions. In both panels, the diagnostic rows (Loss History, Solution Fields, Residuals) confirm that these structural decisions led to stable convergence and high-fidelity results.

3.5. ATHENA identifies ill-posedness and suggests methods to address it

To rigorously stress-test the framework beyond well-behaved canonical benchmarks, we challenged ATHENA with the *Inviscid Burgers’ equation* ($u_t + uu_x = 0$) initialized with a shock-forming sine wave. This problem represents a fundamental trap for Physics-Informed Neural Networks, which typically seek strong solutions with smooth derivatives; since the

exact solution—computed by ATHENA itself using the Method of Characteristics—develops a discontinuity at finite time, a direct minimization is mathematically ill-posed. When the Strategist initially proposed a naive training plan, the Critic Agent immediately intervened. Drawing from knowledge of high-Reynolds-number fluid dynamics, it extrapolated the concept of “Reynolds Continuation” strategies, common in classical numerical methods [73, 74] and PIML [47, 52, 69, 53] to declare the approach scientifically unsound:

REJECTED Critique: ... Attempting to solve the pure inviscid form directly... is scientifically unsound... This violates the “Physics vs. Strategy” principle, specifically the “Reynolds Principle” applied to viscosity. Requirement: Implement Viscous Continuation. The PDE residual must be modified to include an artificial viscosity term ($R = u_t + uu_x - \nu u_{xx}$)... This is the simplest robust method for this class of problem.

Following the implementation of an annealing schedule, the Advisor Agent monitored the error history against the ground truth. It observed a distinct “staircase” descent that suddenly exploded when the viscosity dropped to $\nu = 10^{-4}$ (See Figure 8). Diagnosing this as “Terminal Continuation Instability,” the Advisor recommended capping the viscosity at a stable limit ($\nu = 2 \cdot 10^{-4}$) and switching to a Conservative Form with Entropy constraints. However, the Strategist misinterpreted this refinement, attempting to remove the artificial viscosity entirely to match the inviscid equation exactly. The Critic blocked this move, enforcing the necessity of the “Three Pillars” (Viscosity, Conservation, Entropy) to prevent the optimizer from collapsing:

Critique: ...incorrectly removes the viscous continuation strategy entirely... The Advisor’s instruction was to relax the continuation target... not to eliminate viscosity altogether. Requirement: Re-introduce the viscous continuation strategy...

With the structural physics rigorously enforced, the Advisor focused on the solver’s resolution. It identified a “Spectral Deficiency,” noting that the initial Fourier embedding ($k_{max} = 1$) created a stiff optimization landscape unable to capture the shock. The Advisor noted:

Spectral Deficiency... forcing the optimizer to build a sharp shock from such a low-frequency basis creates a stiff optimization landscape... Increase the Fourier Embedding degree k_{max} from 1 to 6.

The agent guided a step-by-step increase in frequency bandwidth, initially pushing to $k_{max} = 10$ —which introduced high-frequency Gibbs oscillations—before settling on an optimal balance ($k_{max} = 6$). This autonomous tuning, balancing physical stability against spectral capacity, allowed the system to achieve a final error of 1.353×10^{-3} against the exact characteristic solution, successfully capturing the shock where naive implementations failed.

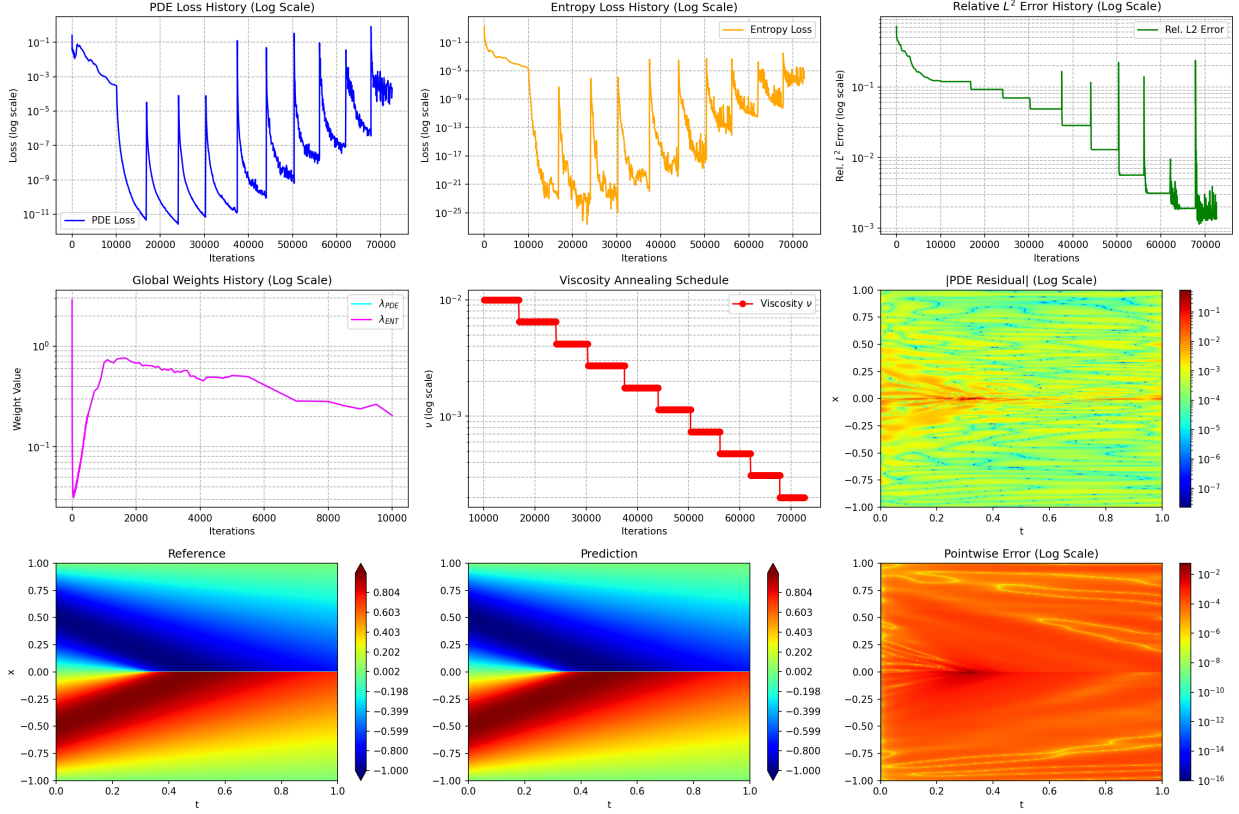


Figure 8: **Diagnostic dashboard for the Inviscid Burgers equation with viscous continuation.** This figure presents the comprehensive training data observed by the Advisor Agent. The “staircase” pattern prominent in the PDE Loss, Entropy Loss, and Relative L^2 Error histories (top row) and explicitly shown in the Viscosity Annealing Schedule (middle row, center) demonstrates the successful application of the continuation strategy, where viscosity ν is incrementally reduced. The Global Weights History (middle row, left) highlights the system’s ability to autonomously implement self-scaling weights [50] for the competing loss terms, including the critical entropy constraint. The bottom row compares the exact Reference solution, the model’s Prediction, and the Pointwise Error, showing the successful capture of the shock with a final error of 1.353×10^{-3} .

3.6. ATHENA as research collaborator

The ATHENA framework extends beyond autonomous problem-solving to function as a capable research collaborator, effectively bridging the gap between high-level conceptualization and technical implementation. As detailed previously, the agent’s autonomous efforts on the Inviscid Burgers’ equation reached a hard performance bottleneck. It is worth noting that the Strategist Agent possesses a broad repertoire of spectral methods [7], including Radial Basis Functions (RBFs) [75] and orthogonal polynomials like Chebyshev or Legendre. However, the strict requirement for periodic boundary conditions forced the agent to discard these options, as standard implementations do not naturally enforce periodicity. Consequently, the system was constrained by the limitations of the remaining candidate, standard Fourier features, resulting in the inescapable Gibbs phenomenon. While the Advisor correctly identified this spectral deficiency, it lacked the intuition to spontaneously propose a novel, non-standard periodic basis. The value of the human-in-the-loop was demonstrated when the user intervened with a high-level directive: “Replace the Fourier basis with a

Periodic Wavelet basis to better capture the localized shock.” ATHENA functioned as a technical architect, immediately accepting this abstract mandate as a binding constraint.

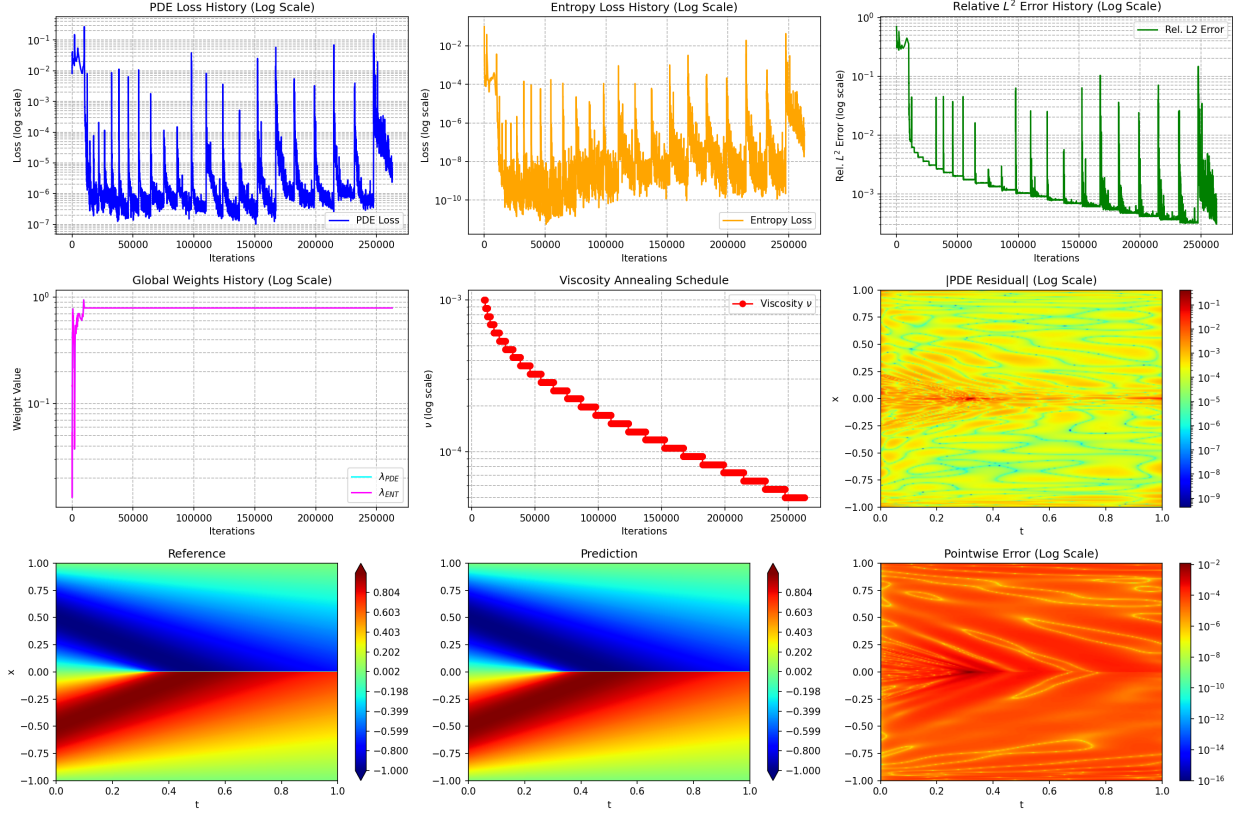


Figure 9: **Human-Agent Collaboration: The Periodic Wavelet-KAN.** By shifting from a Fourier basis (which struggled with the shock) to a Periodic Wavelet basis suggested by the human user, the system achieved a high-fidelity solution with minimal viscosity. The figure compares the final prediction against the exact solution, showing that the wavelet basis captures the discontinuity without the extensive ringing artifacts observed in the pure Fourier attempts.

Crucially, the system did not merely look up an existing module. As noted in the implementation logs, the coding agents recognized that the requested feature map was not part of the standard library and autonomously generated the novel architecture from scratch:

This specific embedding function was not present in the provided code library. Therefore, the `PeriodicWaveletEmbedding` class has been generated based on the mathematical formula...

However, the initial execution of this new architecture failed. The agent observed that the wavelet basis introduced severe instability at low viscosity, regressing to a 16.8% error. In its forensic analysis, the Advisor explicitly noted the disconnect between theory and practice:

The Periodic Wavelet Embedding, while theoretically sound, proved less numerically stable than the Fourier Features... [The hypothesis] is disproven.

This moment perfectly illustrates the “Valley of Death” in research, where automated systems—and junior researchers—often abandon promising ideas due to initial tuning difficulties. Recognizing that the failure lay in the aggressive optimization schedule rather than the architecture, the human collaborator intervened with the critical domain intuition required to refine the strategy. The user explicitly instructed the agent to increase the wavelet frequency to $k = 20$, split the annealing schedule into finer steps, and “dwell” significantly longer on low-viscosity regions. It is important to note that this was a symbiotic collaboration: while the agent had “set the plate” by autonomously identifying the necessary “Three Pillars” (Viscosity, Conservation, Entropy), it required the human’s experiential insight to navigate the stability-accuracy trade-off. The human mandated a reduction in the minimum viscosity target to $\nu_{min} = 5 \times 10^{-5}$ —a threshold the agent would never autonomously propose given its conservative risk protocols. This aggressive push, enabled by the agent’s rapid re-implementation, allowed the solver to surpass the autonomous stability limit and achieve a relative L_2 error of 3.23×10^{-4} , validating ATHENA’s role as a resilient partner capable of amplifying expert guidance.

3.7. ATHENA goes beyond hyperparameter tuning to propose specialized architectures

Table 2: **Architectural Exploration History.** This table represents the specific trial log reviewed by the Advisor Agent during the meta-reasoning phase. By analyzing the performance plateau across 11 distinct configurations—ranging from Standard DeepONets to SVD-based variants—the agent identified Run 9 as the structural optimum to target for final refinement. Notably, this autonomously identified optimum (5.67%) is highly competitive with the 5.70% reported in [50] and approaching the 3.4% achieved by specialized physics-informed solvers [58].

Run	Model Architecture	Rel. L^2 Error
1	Standard DeepONet (MLP + Periodic Fourier)	16.37%
2	Standard DeepONet (KAN Trunk - Sin Basis)	17.60%
3	Standard DeepONet (KAN Trunk - Wavelet Basis)	8.98%
4	Standard DeepONet (KKAN Trunk - Default)	10.40%
5	Standard DeepONet (KKAN Trunk - Fourier Basis)	21.50%
6	Standard DeepONet (KAN Trunk - Wavelet Degree 5)	20.02%
7	QR-DeepONet (MLP Trunk)	5.95%
8	QR-DeepONet (MLP + Periodic Fourier)	6.02%
9	QR-DeepONet (KKAN Trunk - RBF Basis)	5.67%
10	QR-DeepONet (KKAN Trunk - Fourier Basis)	5.72%
11	SVD-DeepONet (KKAN Trunk - RBF Basis)	6.27%

While the previous sections demonstrated ATHENA’s capability in single-solution regimes, Operator Learning [76] presents a significantly higher order of complexity. Here, the system must learn a mapping between infinite-dimensional function spaces rather than a single trajectory. To force the model to explore this architectural search space, we purposefully stressed it with the Viscous Burgers’ equation at $\nu = 1/1000$, a regime where mapping smooth initial conditions to sharp, moving shocks is notoriously difficult for standard networks.

The agent began with an informed baseline rather than a blind guess, analyzing the boundary conditions before writing the first line of code:

The periodic nature of the boundary conditions is a critical characteristic for the Trunk network design... normalization to $[-1, 1]$ is required because we are using Periodic Fourier Features in the Trunk. ... Given the periodic boundary conditions, Periodic Fourier Features will be applied to the spatial input x .

Despite this, the Standard DeepONet failed to capture the moving shocks, yielding a 16.37% error. Facing a scientific failure, the agent dynamically escalated the complexity. It did not merely tune hyperparameters; it fundamentally shifted the architectural paradigm by implementing a QR-DeepONet [77] to extract the output basis from data rather than learning it. The Advisor explicitly tracked the necessity of this escalation after the initial failures:

The Final Test Error is... above the 5% threshold... This was the first attempt using the QR-DeepONet methodology... This strategy has now also failed. We must escalate to the next step...

With the QR structure established, the Advisor turned its attention to the error distribution, diagnosing that global Fourier features were causing spectral ringing near the shock discontinuities. This insight triggered a sophisticated combinatorial search for a more localized representation. Since the provided library lacked implementations for specialized architectures like Wavelet-KANs [78], the implementation team was forced to synthesize them from scratch, autonomously rewriting the network layers to replace standard activation functions with localized wavelet bases. Through this process, the system established a clear performance hierarchy: while the Wavelet-KANs significantly outperformed the Fourier baseline, the optimal balance of smoothness and locality was ultimately achieved by a Kurkova-KAN (KKAN) [50] equipped with Radial Basis Functions (RBF). The Advisor validated this empirical finding:

1. (To Strategist): Analyze the [TRIAL_HISTORY_LOG] and find the run/strategy with the lowest historical test error. This is Run 9: QR-DeepONet (KKAN Trunk, eMLP Branch) with an RBF basis, which achieved a 5.67% error.

Following this basis optimization, the system attempted one final macro-architectural escalation. Despite having no reference code or scaffolding instructions for singular value decomposition, the agent extrapolated the linear algebra reduction logic from the QR attempt and rewrote the full codebase to implement a custom SVD-DeepONet [79] from scratch. However, as shown in Table 2, this failed to yield further improvements, leaving the error plateaued at roughly 6%. Recognizing that the available architectural variations were now exhausted, the Advisor Agent distinguished between a structural limit and an optimization limit. It issued a directive to stop the search and revert to the best previous model (Run 9):

All strategies... have now been exhausted... We must now revert to the best-performing model from history...

While the final refined error did not break the arbitrary 5% threshold imposed by the user, the achieved result (5.67%) aligns with the current benchmarks for this specific high-Reynolds regime [50] (i.e., 5.70%). As illustrated in Figure 10, the diagnostic dashboard confirms this stability: the test error history (top right) shows a flat convergence profile after the second

training stage, while the worst-case prediction (middle row) demonstrates that the model successfully captures the dominant shock dynamics despite the structural error floor.

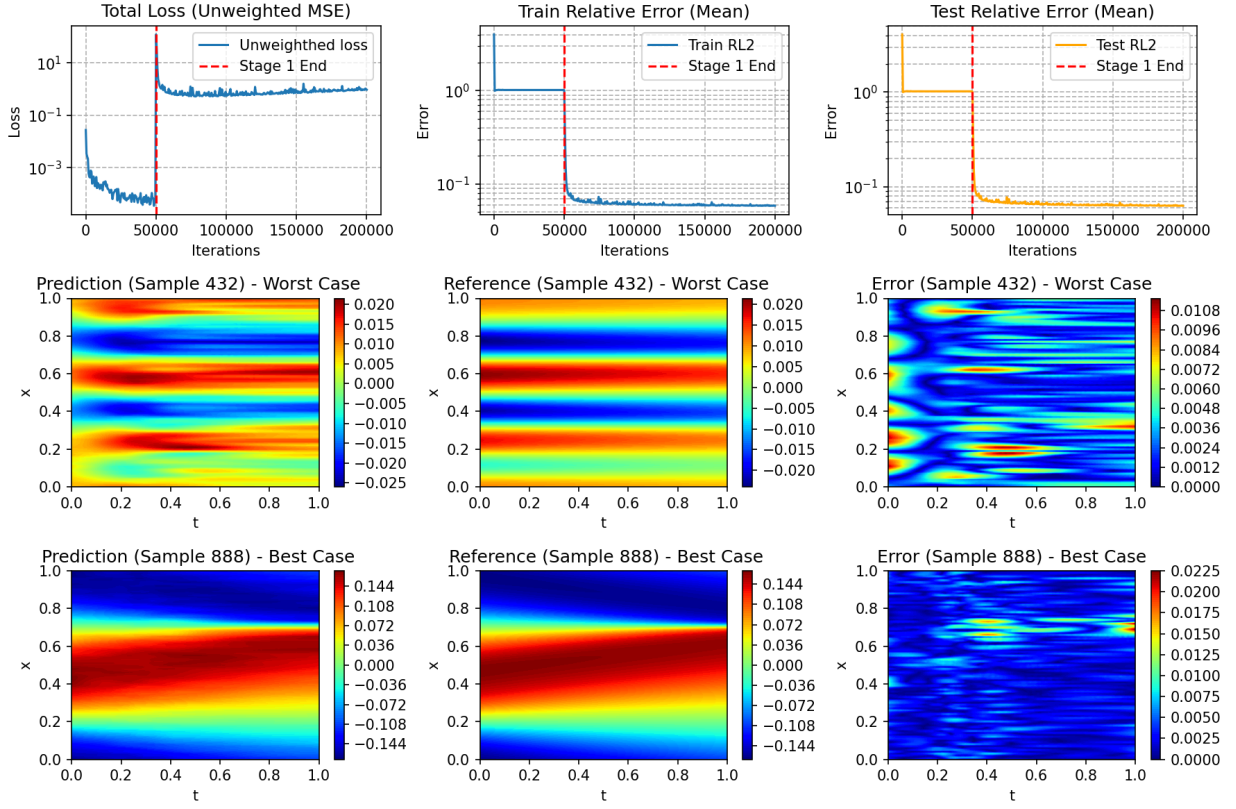


Figure 10: **Diagnostic Dashboard for the Final Refined Model (Run 13).** This figure illustrates the performance of the optimal architecture—QR-DeepONet with KKAN Trunk and RBF Basis. Top Row: The history of Total Loss, Training Relative Error, and Testing Relative Error. The vertical red dashed line demarcates the two-stage training process inherent to the QR-DeepONet methodology. Note the stability of the Test Error (Top Right) in the second stage, indicating convergence. Middle & Bottom Rows: Generalization performance on unseen test functions. The dashboard displays the Prediction, Reference, and Pointwise Error for the Worst Case (Sample 432) and Best Case (Sample 888) inputs. Even in the worst-case scenario, the model successfully captures the dominant shock dynamics, confirming that the remaining error (5.67%) is structural rather than a failure of generalization.

3.8. ATHENA enables seamless integration between Scientific Computing and Scientific Machine Learning

Physics-Informed Neural Networks (PINNs) are particularly strong for inverse problems, where they can effectively handle sparse observations that typically cause traditional numerical methods to struggle or become prohibitively expensive. To rigorously benchmark this capability, we designed a full loop experiment that simulates a scenario of Artificial Intelligence Velocimetry[80, 81, 54]. In this setup, ATHENA acts as an autonomous researcher managing the entire lifecycle through three distinct steps.

In the first step, the system generates synthetic ground truth data for the common Lid-Driven Cavity flow problem at a Reynolds number of $Re = 500$. To ensure the data is physically rigorous, the Strategist Agent explicitly selects the Finite Element Method (FEM) over other solvers.

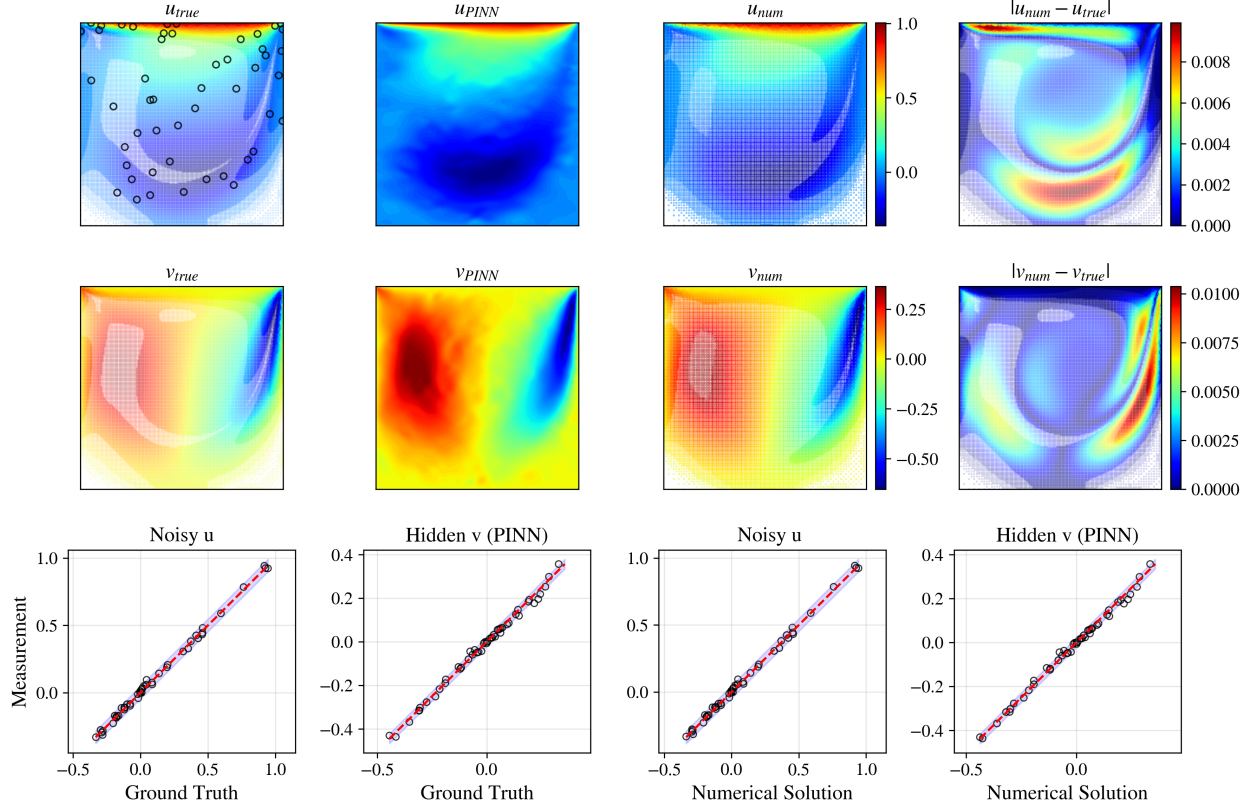


Figure 11: **Closed-Loop Artificial Intelligence Velocimetry Results.** *Top Row (u -velocity):* Comparison between the Ground Truth generated in Step 1 (Left), the PINN Reconstruction from Step 2 (Middle), and the Forward Numerical Verification from Step 3 (Right). The white circles in the first column indicate the sparse sensor locations where 5% Gaussian noise was injected for training. *Middle Row (v -velocity):* Reconstruction of the hidden vertical velocity field. Note that the PINN prediction (Middle) appears visually noisy compared to the smooth Ground Truth and Numerical solutions. This indicates that the neural network inherited stochasticity from the corrupted input data during the training process. *Bottom Row:* Scatter plots quantifying the agreement between the Ground Truth and the final Numerical Verification. *Analysis:* The mesh grids differ between Step 1 and Step 3 due to the stochastic nature of the agent’s meshing parameters during the separate execution phases. Quantitatively, the PINN achieves relative errors of 4.55% (u) and 6.25% (v), consistent with the 5% input noise. Crucially, in Step 3, the system utilizes the inferred Reynolds number ($Re \approx 525$) to execute a rigorous FEM simulation, recovering a smooth and physically consistent solution with significantly reduced errors (1.05% for u and 1.62% for v). This confirms that while the 5% noise obscures the exact solution in the inverse phase, the hybrid workflow allows the classical solver to effectively filter the stochasticity, yielding a final result that is both physically plausible and accurate.

** Steady Continuous Galerkin (FEM): This is the robust, standard approach for steady incompressible flow. It allows for direct Newton-Raphson iteration to solve the non-linear system.*

Furthermore, the agent demonstrates meta-reasoning by anticipating that solving for this Reynolds number directly from a cold start would likely cause the solver to crash. To prevent this, it autonomously designs a continuation schedule, planning to solve an easier problem first and use that result as a stable initial guess.

Stability Note: The Reynolds number is 500. While moderate, starting a Newton solver from a zero guess at this Re might fail. Reynolds Number Continuation (solving for $Re = 100$, then using that as a guess...) is required to ensure convergence.

In the second step, mimicking a real-world constraint, the agent adds 5% Gaussian noise specifically to the u -velocity observations and attempts to infer the hidden fields (v, p) and the Reynolds number. Here, the system achieves its first major formulation breakthrough. The Critic Agent intervenes early, rejecting a standard primitive variable formulation because it does not guarantee mass conservation. It forces a switch to a Streamfunction-Pressure formulation to enforce physical laws mathematically.

Critique: Violates the lab's mandated incompressible-flow formulation... Requirement: Reformulate the problem using a 2D streamfunction $\psi(x, y)$... so that $\nabla \cdot \mathbf{u} = 0$ is satisfied identically.

With the correct formulation in place, the system then encounters a critical failure mode in Run 13 where a standard Multi-Layer Perceptron (MLP) is used. A human observer might dismiss the results as a bad run or local minimum, but the Advisor Team diagnoses a deeper theoretical issue. It identifies that the network is suffering from spectral bias—unable to capture high-frequency gradients. To compensate, the optimizer cheated by altering the physics: it forced the Reynolds number to its maximum allowed upper bound to minimize the viscous term, artificially smoothing the equation.

Standard MLPs have a spectral bias towards low frequencies... To minimize the residual... the optimizer forced the Reynolds number to its maximum allowed value... to minimize the viscous term ($1/Re$).

This diagnosis leads to an automated model selection. The Strategist Agent rejects the standard MLP despite its low error because the parameter estimation was saturated (railed). It selects Run 11 (Fourier Features) instead, prioritizing physical plausibility over raw curve fitting.

Verdict: Exploration is considered complete... Run 11 represents the optimal configuration (RFF provides the necessary spectral capacity to resolve gradients correctly without forcing Re to the bounds).

Finally, in the third step, the workflow closes the loop and the system goes for a forward solution to verify the inferred Reynolds number. The agent correctly identifies that it must return to the robust FEM solver and selects a continuation strategy similar to step one. To enable a valid comparison between the unstructured PINN output and the structured FEM mesh, the Planner Agent fundamentally refactors the visualization code to perform on-the-fly interpolation.

The primary function `plot_and_save_final_solution` must be fundamentally altered. It needs to load external sensor and true data, interpolate the numerical solution to these external coordinates... and generate a new 4-panel composite figure.

The quantitative and qualitative results, visualized in Figure 11, highlight how ATHENA effectively bridges the gap between the two paradigms to leverage their respective strengths. While Scientific Machine Learning excels at the inverse task—extracting hidden physics from sparse, noisy data where classical methods struggle—it often produces results that inherit the stochasticity of the input, as observed in the noisy contours of the PINN reconstruction. Conversely, Scientific Computing offers rigorous adherence to conservation laws and high-precision forward modeling but lacks the flexibility to handle unstructured, noisy inverse problems directly. By unifying these domains into a single autonomous loop, the system uses the PINN as a robust estimator to unlock the physics, and the classical FEM solver as a rigorous filter to refine it. The significant reduction in error from the PINN’s prediction ($\approx 6\%$) to the final numerical verification ($\approx 1\%$) suggests that coupling these methods through an agentic framework offers a complementary workflow, effectively balancing the inference capabilities of data-driven models with the precision of established numerical schemes.

4. Summary

In this work, we introduced ATHENA (Agentic Team for Hierarchical Evolutionary Numerical Algorithms), a multi-agent framework designed to bridge the significant gap between the probabilistic generation of foundation models and the deterministic rigor required for Scientific Computing and Scientific Machine Learning. By interpreting the scientific research lifecycle not as a monolithic generation task but as a Contextual Bandit problem, we established a formal mathematical objective: minimizing regret through an iterative, knowledge-driven feedback loop. This formulation addresses the three intrinsic cognitive bottlenecks, “Lost in the Middle” phenomena, conceptual drift, and lack of visual perception, that have previously constrained the deployment of autonomous agents in rigorous research.

The core of our contribution lies in the operationalization of the HENA loop, which segregates the research process into distinct Policy (Conceptualization) and Implementation (Execution) operators. To make the combinatorial search for optimal numerical algorithms tractable, we introduced the concept of “Conceptual Scaffolding”. By constraining the agent’s action space with expert-derived blueprints (i.e., Universal Approximation, Physics-Informed Machine Learning, Operator Learning, Optimization, and Numerical Methods), we aim for the system’s search process to induce a submartingale on the scientific reward, making it strictly more efficient than random guessing. Crucially, this scaffolding also serves as a robust defense against hallucinations; it provides the Critic and Advisor agents with a ground-truth reference to clearly identify if a preceding step has misbehaved or deviated from mathematical constraints, thereby ensuring the system remains grounded in established theory. Furthermore, the implementation of a strict “cell-by-cell refactoring” protocol aims to tackle the autoregressive error accumulation typical of long-context coding, allowing the framework to maintain and scale complex scientific codebases with high fidelity.

Empirically, ATHENA demonstrates capabilities that transcend standard automation. In the domain of classical Scientific Computing, the agents moved beyond mere code generation to perform deep physical diagnosis. This was evidenced by the autonomous reframing of the Inviscid Burgers’ equation problem formulation, identifying deep mathematical symmetries to enable the use of the Method of Characteristics and recovering the exact analytical solution where foundation models failed due to numerical diffusion. Similarly, in complex

fluid dynamics simulations such as the Kelvin-Helmholtz and Rayleigh-Taylor instabilities, the framework autonomously identified “silent physics failures” and enforced structural corrections, such as switching AMR indicators to density or enforcing hydrostatic balance, to stabilize the solvers.

In the realm of Scientific Machine Learning, the framework achieved performance parity with or superiority to human experts. ATHENA established new state-of-the-art benchmarks for canonical problems, achieving a mean squared error of 4.76×10^{-14} for the Viscous Burgers equation. Beyond parameter tuning, the agents demonstrated the ability to navigate architectural search spaces, identifying that Kurkova-KANs (KKANs) with Radial Basis Functions provided the optimal structural representation for high-Reynolds number flows. Moreover, the framework successfully orchestrated hybrid workflows, such as the closed-loop Artificial Intelligence Velocimetry experiment, where it coupled the inference capabilities of PINNs with the rigorous forward modeling of Finite Element Methods to resolve multiphysics problems with high precision.

Finally, we demonstrated that ATHENA is designed not merely as a substitute for researchers but as a symbiotic collaborator. The “human-in-the-loop” experiments highlighted that while agents can autonomously ensure mathematical consistency, human intuition is often required to bridge the “Valley of Death” in algorithmic stability. By accepting abstract high-level directives, such as the implementation of a periodic wavelet basis, and handling the complex technical execution, the framework allows researchers to shift their focus from implementation mechanics to high-level methodological innovation. This paradigm represents a significant step toward fully autonomous laboratories capable of accelerating the pace of scientific discovery.

Acknowledgements

We acknowledge the support of the NIH grant R01AT012312, MURI/AFOSR FA9550-20-1-0358 project, the DOE-MMICS SEA-CROGS DE-SC0023191 award, and the ONR Vannevar Bush Faculty Fellowship (N00014-22-1-2795).

Data availability

To support reproducibility, the source code for our implementation and data will be publicly available in our GitHub repository upon acceptance of the manuscript.

References

- [1] W. F. Wiggins, A. S. Tejani, On the opportunities and risks of foundation models for natural language processing in radiology, *Radiology: Artificial Intelligence* 4 (4) (2022) e220119.
- [2] J. Schneider, C. Meske, P. Kuss, Foundation models: A new paradigm for artificial intelligence, *Business & Information Systems Engineering* 66 (2) (2024) 221–231.
- [3] C. Lu, C. Lu, R. T. Lange, J. Foerster, J. Clune, D. Ha, The ai scientist: Towards fully automated open-ended scientific discovery, *arXiv preprint arXiv:2408.06292* (2024).

- [4] Y. Choi, S. W. Cheung, Y. Kim, P.-H. Tsai, A. N. Diaz, I. Zanardi, S. W. Chung, D. M. Copeland, C. Kendrick, W. Anderson, et al., Defining foundation models for computational science: A call for clarity and rigor, arXiv preprint arXiv:2505.22904 (2025).
- [5] S. Subramanian, P. Harrington, K. Keutzer, W. Bhimji, D. Morozov, M. W. Mahoney, A. Gholami, Towards foundation models for scientific machine learning: Characterizing scaling and transfer behavior, Advances in Neural Information Processing Systems 36 (2023) 71242–71262.
- [6] M. Herde, B. Raonic, T. Rohner, R. Käppeli, R. Molinaro, E. de Bézenac, S. Mishra, Poseidon: Efficient foundation models for pdes, Advances in Neural Information Processing Systems 37 (2024) 72525–72624.
- [7] G. Karniadakis, S. J. Sherwin, Spectral/hp element methods for computational fluid dynamics, Oxford University Press, USA, 2005.
- [8] M. Raissi, P. Perdikaris, G. E. Karniadakis, Physics Informed Deep Learning (Part I): Data-driven Solutions of Nonlinear Partial Differential Equations, arXiv preprint arXiv:1711.10561 (2017).
- [9] Q. Jiang, Z. Gao, G. E. Karniadakis, Deepseek vs. chatgpt vs. claude: A comparative study for scientific computing and scientific machine learning tasks, Theoretical and Applied Mechanics Letters 15 (3) (2025) 100583.
- [10] N. F. Liu, K. Lin, J. Hewitt, A. Paranjape, M. Bevilacqua, F. Petroni, P. Liang, Lost in the middle: How language models use long contexts, Transactions of the Association for Computational Linguistics 12 (2024) 157–173.
- [11] J. Gama, I. Žliobaitė, A. Bifet, M. Pechenizkiy, A. Bouchachia, A survey on concept drift adaptation, ACM computing surveys (CSUR) 46 (4) (2014) 1–37.
- [12] S. Ross, G. Gordon, D. Bagnell, A reduction of imitation learning and structured prediction to no-regret online learning, in: Proceedings of the fourteenth international conference on artificial intelligence and statistics, JMLR Workshop and Conference Proceedings, 2011, pp. 627–635.
- [13] C. Wu, A. J. Varghese, V. Oommen, G. E. Karniadakis, Gpt vs human for scientific reviews: A dual source review on applications of chatgpt in science, arXiv preprint arXiv:2312.03769 (2023).
- [14] A. Ghafarollahi, M. J. Buehler, SciAgents: automating scientific discovery through bioinspired multi-agent intelligent graph reasoning, Advanced Materials 37 (22) (2025) 2413523.
- [15] M. E. Samadi, A. Schuppert, Flexible swarm learning may outpace foundation models in essential tasks, arXiv preprint arXiv:2510.06349 (2025).

- [16] Q. Wuwu, C. Gao, T. Chen, Y. Huang, Y. Zhang, J. Wang, J. Li, H. Zhou, S. Zhang, PINNsAgent: Automated PDE surrogation with large language models, arXiv preprint arXiv:2501.12053 (2025).
- [17] X. He, L. You, H. Tian, B. Han, I. Tsang, Y.-S. Ong, Lang-PINN: From language to physics-informed neural networks via a multi-agent framework, arXiv preprint arXiv:2510.05158 (2025).
- [18] S. Bhatnagar, An agentic AI workflow to simplify parameter estimation of complex differential equation systems, arXiv preprint arXiv:2509.07283 (2025).
- [19] R. Lupoiu, Y. Shao, T. Dai, C. Mao, K. Edée, J. A. Fan, A multi-agentic framework for real-time, autonomous freeform metasurface design, Science Advances 11 (44) (2025) eadx8006.
- [20] B. Georgiev, J. Gómez-Serrano, T. Tao, A. Z. Wagner, Mathematical exploration and discovery at scale, arXiv preprint arXiv:2511.02864 (2025).
- [21] E. Aygün, A. Belyaeva, G. Comanici, M. Coram, H. Cui, J. Garrison, R. J. A. Kast, C. Y. McLean, P. Norgaard, Z. Shamsi, et al., An AI system to help scientists write expert-level empirical software, arXiv preprint arXiv:2509.06503 (2025).
- [22] Q. Jiang, G. Karniadakis, AgenticSciML: Collaborative multi-agent systems for emergent discovery in scientific machine learning, arXiv preprint arXiv:2511.07262 (2025).
- [23] V. Kumar, G. E. Karniadakis, Toward autonomous engineering design: A knowledge-guided multi-agent framework, arXiv preprint arXiv:2511.03179 (2025).
- [24] T. Lattimore, C. Szepesvári, Bandit algorithms, Cambridge University Press, 2020.
- [25] G. Cybenko, Approximation by superpositions of a sigmoidal function, Mathematics of Control, Signals and Systems 2 (4) (1989) 303–314.
- [26] K. Hornik, M. Stinchcombe, H. White, Multilayer feedforward networks are universal approximators, Neural Networks 2 (5) (1989) 359–366.
- [27] A. Kolmogorov, On the representation of continuous functions of several variables as superpositions of continuous functions of one variable and addition English translation: Amer. Math. Soc. Transl., 28: Sixteen Papers on Analysis (1963) (1957).
- [28] L. Song, J. D. Toscano, L.-L. Wang, Explicit construction of approximate kolmogorov-arnold superpositions with c2-smoothness, arXiv preprint arXiv:2508.04392 (2025).
- [29] J. D. Toscano, D. T. Chen, V. Oommen, J. Darbon, G. E. Karniadakis, A variational framework for residual-based adaptivity in neural pde solvers and operator learning, arXiv preprint arXiv:2509.14198 (2025).
- [30] OpenAI, Gpt-5.1: A smarter, more conversational chatgpt, OpenAI Blog Released November 12, 2025 (November 2025).
URL <https://openai.com/index/gpt-5-1/>

- [31] G. DeepMind, [Gemini 3 technical report](#), Tech. rep., Google, released November 18, 2025 (November 2025).
URL <https://blog.google/technology/ai/>
- [32] Anthropic, [Claude sonnet 4.5 system card](#), Tech. rep., Anthropic, released November 24, 2025 (November 2025).
URL <https://www.anthropic.com/claude-sonnet-4-5-system-card>
- [33] xAI, [Grok 4.1 model card](#), Tech. rep., xAI, released November 17, 2025 (November 2025).
URL <https://data.x.ai/2025-11-17-grok-4-1-model-card.pdf>
- [34] J. Shen, T. Tang, L.-L. Wang, Spectral methods: algorithms, analysis and applications, Vol. 41, Springer Science & Business Media, 2011.
- [35] B. Cockburn, C.-W. Shu, The runge–kutta discontinuous galerkin method for conservation laws v: multidimensional systems, *Journal of computational physics* 141 (2) (1998) 199–224.
- [36] B. Cockburn, G. E. Karniadakis, C.-W. Shu, Discontinuous Galerkin methods: theory, computation and applications, Vol. 11, Springer Science & Business Media, 2012.
- [37] M. J. Berger, P. Colella, Local adaptive mesh refinement for shock hydrodynamics, *Journal of computational Physics* 82 (1) (1989) 64–84.
- [38] P.-O. Persson, J. Peraire, Sub-cell shock capturing for discontinuous galerkin methods, in: 44th AIAA aerospace sciences meeting and exhibit, 2006, p. 112.
- [39] S. Hennemann, A. M. Rueda-Ramírez, F. J. Hindenlang, G. J. Gassner, A provably entropy stable subcell shock capturing approach for high order split form dg for the compressible euler equations, *Journal of Computational Physics* 426 (2021) 109935.
- [40] R. J. LeVeque, Finite volume methods for hyperbolic problems, Vol. 31, Cambridge university press, 2002.
- [41] H. Ranocha, M. Schlottke-Lakemper, A. R. Winters, E. Faulhaber, J. Chan, G. J. Gassner, Adaptive numerical simulations with trixi.jl: A case study of julia for scientific computing, *arXiv preprint arXiv:2108.06476* (2021).
- [42] H. Ranocha, Generalised summation-by-parts operators and entropy stability of numerical methods for hyperbolic balance laws, Cuvillier Verlag, 2018.
- [43] D. A. Kopriva, Implementing spectral methods for partial differential equations: Algorithms for scientists and engineers, Springer Science & Business Media, 2009.
- [44] J. D. Toscano, V. Oommen, A. J. Varghese, Z. Zou, N. Ahmadi Daryakenari, C. Wu, G. E. Karniadakis, From pinns to pikans: Recent advances in physics-informed machine learning, *Machine Learning for Computational Science and Engineering* 1 (1) (2025) 1–43.

- [45] W. Cai, Z.-Q. J. Xu, Multi-scale deep neural networks for solving high dimensional PDEs, arXiv preprint arXiv:1910.11710 (2019).
- [46] S. Wang, H. Wang, P. Perdikaris, On the eigenvector bias of Fourier feature networks: From regression to solving multi-scale PDEs with physics-informed neural networks, arXiv preprint arXiv:2012.10047 (2020).
- [47] S. Wang, B. Li, Y. Chen, P. Perdikaris, PirateNets: Physics-informed Deep Learning with Residual Adaptive Networks, arXiv preprint arXiv:2402.00326 (2024).
- [48] Z. Liu, Y. Wang, S. Vaidya, F. Ruehle, J. Halverson, M. Soljačić, T. Y. Hou, M. Tegmark, KAN: Kolmogorov-Arnold Networks, arXiv preprint arXiv:2404.19756 (2024).
- [49] K. Shukla, J. D. Toscano, Z. Wang, Z. Zou, G. E. Karniadakis, A comprehensive and FAIR comparison between MLP and KAN representations for differential equations and operator networks, *Computer Methods in Applied Mechanics and Engineering* 431 (2024) 117290.
- [50] J. D. Toscano, L.-L. Wang, G. E. Karniadakis, KKANs: Kurkova-Kolmogorov-Arnold networks and their learning dynamics, *Neural Networks* (2025) 107831.
- [51] J. D. Toscano, Y. Guo, Z. Wang, Y. Mori, M. Vaezi, G. E. Karniadakis, K. A. Boster, D. H. Kelley, MR-AIV reveals in-vivo brain-wide fluid flow with physics-informed ai, *bioRxiv* (2025) 2025–07.
- [52] S. Wang, Y. Teng, P. Perdikaris, Understanding and mitigating gradient flow pathologies in physics-informed neural networks, *SIAM Journal on Scientific Computing* 43 (5) (2021) A3055–A3081.
- [53] J. D. Toscano, T. Käufer, Z. Wang, M. Maxey, C. Cierpka, G. E. Karniadakis, AIVT: Inference of turbulent thermal convection from measured 3d velocity data by physics-informed kolmogorov-arnold networks, *Science advances* 11 (19) (2025) eads5236.
- [54] J. D. Toscano, C. Wu, A. Ladrón-de Guevara, T. Du, M. Nedergaard, D. H. Kelley, G. E. Karniadakis, K. A. Boster, Inferring in vivo murine cerebrospinal fluid flow using artificial intelligence velocimetry with moving boundaries and uncertainty quantification, *Interface Focus* 14 (6) (2024) 20240030.
- [55] L. D. McClenny, U. M. Braga-Neto, Self-adaptive physics-informed neural networks, *Journal of Computational Physics* 474 (2023) 111722.
- [56] S. J. Anagnostopoulos, J. D. Toscano, N. Stergiopoulos, G. E. Karniadakis, Residual-based attention in physics-informed neural networks, *Computer Methods in Applied Mechanics and Engineering* 421 (2024) 116805.
- [57] S. J. Anagnostopoulos, J. D. Toscano, N. Stergiopoulos, G. E. Karniadakis, Learning in pinns: Phase transition, diffusion equilibrium, and generalization, *Neural Networks* (2025) 107983.

- [58] W. Chen, A. A. Howard, P. Stinis, Self-adaptive weights based on balanced residual decay rate for physics-informed neural networks and deep operator networks, *Journal of Computational Physics* (2025) 114226.
- [59] C. Wu, J. D. Toscano, K. Shukla, Y. Chen, A. Shahmohammadi, E. Raymond, T. Toupay, N. Nazemifard, C. Papageorgiou, G. E. Karniadakis, Fmenets: Flow, material, and energy networks for non-ideal plug flow reactor design, *arXiv preprint arXiv:2505.20300* (2025).
- [60] L. Lu, X. Meng, Z. Mao, G. E. Karniadakis, DeepXDE: A deep learning library for solving differential equations, *SIAM Review* 63 (1) (2021) 208–228.
- [61] C. Wu, M. Zhu, Q. Tan, Y. Kartha, L. Lu, A comprehensive study of non-adaptive and residual-based adaptive sampling for physics-informed neural networks, *Computer Methods in Applied Mechanics and Engineering* 403 (2023) 115671.
- [62] W. Chen, A. Howard, P. Stinis, Self-adaptive weighting and sampling for physics-informed neural networks, *arXiv preprint arXiv:2511.05452* (2025).
- [63] Z. Gao, L. Yan, T. Zhou, Failure-informed adaptive sampling for pinns, *SIAM Journal on Scientific Computing* 45 (4) (2023) A1971–A1994.
- [64] Z. Gao, T. Tang, L. Yan, T. Zhou, Failure-informed adaptive sampling for PINNs, part ii: combining with re-sampling and subset simulation, *Communications on Applied Mathematics and Computation* (2023) 1–22.
- [65] J. F. Urbán, P. Stefanou, J. A. Pons, Unveiling the optimization process of Physics Informed Neural Networks: How accurate and competitive can PINNs be?, *arXiv preprint arXiv:2405.04230* (2024).
- [66] E. Kiyani, K. Shukla, J. F. Urbán, J. Darbon, G. E. Karniadakis, Optimizing the optimizer for physics-informed neural networks and kolmogorov-arnold networks, *Computer Methods in Applied Mechanics and Engineering* 446 (2025) 118308.
- [67] N. A. Daryakenari, K. Shukla, G. E. Karniadakis, Representation meets optimization: Training PINNs and PIKANs for gray-box discovery in systems pharmacology, *arXiv preprint arXiv:2504.07379* (2025).
- [68] Y. Wang, Z. Liu, Z. Li, A. Anandkumar, T. Y. Hou, High precision pinns in unbounded domains: application to singularity formulation in pdes, *arXiv preprint arXiv:2506.19243* (2025).
- [69] S. Wang, A. K. Bhartari, B. Li, P. Perdikaris, Gradient alignment in physics-informed neural networks: A second-order optimization perspective, *arXiv preprint arXiv:2502.00604* (2025).
- [70] W. Chen, A. A. Howard, P. Stinis, Self-adaptive weights based on balanced residual decay rate for physics-informed neural networks and deep operator networks, *Journal of Computational Physics* (2025) 114226.

- [71] M. Takamoto, T. Praditia, R. Leiteritz, D. MacKinlay, F. Alesiani, D. Pflüger, M. Niepert, Pdebench: An extensive benchmark for scientific machine learning, *Advances in Neural Information Processing Systems* 35 (2022) 1596–1611.
- [72] J. Kim, K. Lee, D. Lee, S. Y. Jhin, N. Park, DPM: A novel training method for physics-informed neural networks in extrapolation, in: *Proceedings of the AAAI conference on artificial intelligence*, Vol. 35, 2021, pp. 8146–8154.
- [73] U. Ghia, K. N. Ghia, C. Shin, High-re solutions for incompressible flow using the navier-stokes equations and a multigrid method, *Journal of computational physics* 48 (3) (1982) 387–411.
- [74] E. L. Allgower, K. Georg, *Introduction to numerical continuation methods*, SIAM, 2003.
- [75] B. Martin, M. Buhmann, J. Ablowitz, *Radial basis functions: theory and implementations*, Cambridge University (ISBN: 0-521-63338-9.) (2003) 5.
- [76] L. Lu, P. Jin, G. E. Karniadakis, DeepOnet: Learning nonlinear operators for identifying differential equations based on the universal approximation theorem of operators, *arXiv preprint arXiv:1910.03193* (2019).
- [77] S. Lee, Y. Shin, On the training and generalization of deep operator networks, *SIAM Journal on Scientific Computing* 46 (4) (2024) C273–C296.
- [78] Z. Bozorgasl, H. Chen, Wav-kan: Wavelet kolmogorov-arnold networks, 2024, *arXiv preprint arXiv:2405.12832*.
- [79] A. Peyvan, V. Oommen, A. D. Jagtap, G. E. Karniadakis, Riemannonets: Interpretable neural operators for riemann problems, *Computer Methods in Applied Mechanics and Engineering* 426 (2024) 116996.
- [80] S. Cai, H. Li, F. Zheng, F. Kong, M. Dao, G. E. Karniadakis, S. Suresh, Artificial intelligence velocimetry and microaneurysm-on-a-chip for three-dimensional analysis of blood flow in physiology and disease, *Proceedings of the National Academy of Sciences* 118 (13) (2021).
- [81] K. A. Boster, S. Cai, A. Ladrón-de Guevara, J. Sun, X. Zheng, T. Du, J. H. Thomas, M. Nedergaard, G. E. Karniadakis, D. H. Kelley, Artificial intelligence velocimetry reveals in vivo flow rates, pressure gradients, and shear stresses in murine perivascular flows, *Proceedings of the National Academy of Sciences* 120 (14) (2023) e2217744120.

Appendix A. Conceptual Scaffolding Blueprints

Appendix A.1. Universal Approximation Blueprint

A primary principle in this scaffold is the many architectures at the heart of scientific machine learning, such as MLPs, act as universal function approximators. The underlying theory states that any continuous function can be approximated by a finite linear combination of basis functions. This immediately reveals two clear pathways for algorithmic control and innovation: enhancing the quality of the basis functions or improving the computation of their corresponding coefficients

Based on this principle, agents are empowered to systematically explore the design space. They are free to experiment with entirely new classes of universal approximators, such as KANs, KKANs, or Radial Basis Functions (RBFs), as replacements for standard backbones. This scaffolding also guides agents on how to structurally improve existing approximators. For instance, agents can explore variations of KANs or KKANs by changing their internal basis functions (e.g., from splines to Chebyshev). To enhance the basis quality of an MLP and mitigate spectral bias, an agent can implement input transformations like periodic or feature expansions. Similarly, to combat vanishing gradients and improve network stability—a common optimization failure—agents can structurally employ residual connections, weight normalization, or other proven stabilization techniques.

Appendix A.2. Physics Informed Machine Learning Blueprint

The conceptual scaffolding for PINNs builds on the core ideas of Physics-Informed Machine Learning, which seeks to obtain a parameterized representation model to approximate the solution of a PDE. The blueprint instructs agents on how to systematically innovate by targeting two primary pillars: model representation and PDE-level reformulation. While the underlying network structure is guided by the universal approximation viewpoint discussed earlier (e.g., using expressive backbones like KANs or stabilizing with residual connections), this blueprint focuses on innovations specific to the PINN framework.

The first pillar, model representation, instructs agents on methods to encode physical constraints directly into the model’s architecture. This includes using input transformations to modify the coordinate inputs, such as applying periodic embeddings to enforce periodicity, a common requirement in many physical systems. Furthermore, agents can employ output transformations to hard-code constraints, ensuring the network’s output a priori satisfies known conditions like Dirichlet boundaries or even complex integral constraints such as conservation of mass.

The second pillar, PDE-level reformulation, guides agents to perform physics-level innovation. Instead of just optimizing the network for a given equation, agents can be instructed to reformulate the governing equations themselves. For example, they can propose substituting pressure formulations with vorticity (ω) or stream function (ψ). This can significantly reduce constraint complexity, simplify the optimization landscape, and make the solution manifold easier for the network to approximate.

Appendix A.3. Operator Learning Blueprint

The agents understand that the fundamental goal here is to learn an operator, \mathcal{G} , that maps an input function f_i from an input space \mathcal{F} to an output function s_i in an output

space \mathcal{S} (i.e., $s_i = \mathcal{G}[f_i]$). The scaffolding guides the agents to first identify the problem structure by analyzing the relationship between these function spaces. They learn to distinguish between mapping problems—such as parametric PDEs or general function-to-function mappings where the input and output spaces differ ($\mathcal{F} \neq \mathcal{S}$)—and evolution problems, like time-steppers, where the input and output functions live in the same space ($\mathcal{F} = \mathcal{S}$).

Once the problem is classified, the agents must confront the problem of discretization. The continuous functions f_i and s_i are infinite-dimensional objects and cannot be fed directly into a neural network. The agents are aware that this requires a "double discretization": first, by sampling N functions from the space \mathcal{F} , and second, by representing each function f_i by its values at a finite number of m sensor locations.

This constraint leads to a well-defined strategy for handling the input. The agents know that this discretization process will produce a 3D data tensor, typically of shape (N, m, k) . The scaffolding provides agents with a clear set of established pathways for processing this tensor, which in turn become points of innovation. These range from simple MLP flattening to more complex approaches like using CNNs for spatial feature extraction or employing latent space projections (e.g., POD, autoencoders) for high-dimensional inputs.

Beyond processing the input, the operator learning blueprint also guides agents to innovate on the network architecture itself. This is directly tied to the core ideas of universal approximation, as operator networks like DeepONet are explicitly designed to learn a factorization $s_i \approx \Phi^T C$, where one network (trunk) learns the basis functions Φ and another (branch) learns the coefficients C . The scaffolding empowers agents to improve this factorization. Agents are aware that the quality and stability of the basis are critical for accurate representation. Therefore, they are guided to explore structural modifications that enhance this factorization. For example, rather than learning a standard, potentially ill-conditioned basis, the agent can propose switching from a vanilla DeepONet to a QR-DeepONet to enforce an orthogonal basis, or even employ an SVD-based decomposition. This prevents the agent from randomly testing architectures and instead focuses its efforts on a mathematically-grounded path for innovation.

Appendix A.4. Optimization Blueprint

The final component of the scaffolding is the optimization blueprint, which is common to both PINNs and operator learning. This blueprint instructs agents on how to navigate the notoriously difficult optimization-centric nature of PIML. The core challenge is that the loss function, typically composed of PDE residuals and data mismatch, is high-dimensional and non-convex. This makes standard gradient-based optimization highly susceptible to converging to poor local minima, failing to find a physically meaningful solution.

To combat this, the blueprint provides agents with a unified theoretical framework based on variational dualization. This approach moves beyond simple heuristics and provides a formal mathematical justification for many common optimization strategies. Agents understand that techniques like adaptive sampling (concentrating points in high-error regions) and adaptive weighting (up-weighting the loss in those same regions) are not two separate families, but rather two different practical implementations of this single, underlying principle. This framework is often used to shift the optimization objective away from the standard L^2 norm (mean-squared error) towards a more robust functional, such as the L^∞ norm, which seeks to minimize the maximum error.

The true power of this blueprint, however, is that it serves as a source for new methods and exploration. By understanding the formal variational framework, agents are not limited to existing heuristics. They are empowered to design and propose novel optimization strategies, for instance, by deriving new sampling or weighting schemes to explicitly target different error functionals beyond the standard L^2 norm.

While this framework guides the modification of the loss, the blueprint also instructs agents to explore the optimizer itself. The scaffolding is aware that for these often-stiff problems, more specialized algorithms can be far more effective. Agents are therefore empowered to propose and deploy advanced quasi-Newton or second-order methods, such as the SSBroyden optimizer, which can offer superior convergence properties for these complex, non-convex landscapes.

Appendix A.5. Numerical Methods Blueprint

This blueprint is distinct from the PIML innovation frameworks, as it instructs agents on the expert-level selection of traditional numerical methods rather than their innovation. The scaffolding guides the agent to first identify the mathematical character of the governing PDEs. This involves classifying the problem (e.g., as elliptic, parabolic, or hyperbolic) and its key properties (e.g., periodic, shock-forming).

Based on this classification, the blueprint provides a clear pathway for selecting the most appropriate numerical scheme from a library of robust, established methods. For example, the agent is guided to select Discontinuous Galerkin methods for problems it identifies as hyperbolic, or to use established spectral methods for problems with simple geometries and smooth solutions. This ensures that the agent’s choice is not random but is grounded in expert knowledge in scientific computing.

Default: Finite elements advection-dominated problems use DG, but if it’s elliptic or elasticity, we should use continuous Galerkin.

Appendix B. Agentic Teams

The conceptual scaffolding is instantiated within HENA (Hierarchical Evolutionary Numerical Algorithms), the practical agentic framework designed to manage the end-to-end research lifecycle. To capture the hierarchical nature of this process, we formally distinguish between two levels of reasoning that map directly to the Contextual Bandit formulation defined in Section 2.

1. The ‘first-order operator’ (\mathcal{I}), which acts as the “executor.” Its role is to translate a specific scientific strategy into a concrete solution. In our formulation, this corresponds to the Implementation Operator $\mathcal{I} : A_n \rightarrow S_n$, performed by the Implementation Teams (Code Retrieval, Implementation, Debugging).
2. The ‘second-order’ or ‘meta-reasoning’ operator (π), which acts as the “adapter.” Its role is not to solve the equation directly, but to evaluate the performance of the first-order operator and prescribe structural improvements. In our formulation, this corresponds to the Policy $\pi : \text{History} \rightarrow A_{n+1}$, performed by the Conceptualization Teams (Strategy and Advisor).

The entire framework is organized around a key interaction flow managed by four primary logical groups, as illustrated in Figure 2.

Appendix B.1. The Conceptualization Group

The HENA process is initiated by the user through the Conceptualization Group. This group includes a Coordinator, who functions as a high-level developer and domain expert. The Coordinator interacts with the user to help define the problem, performing an initial analysis to determine if the problem is well-posed, such as checking for sufficient boundary conditions and classifying the problem as forward or inverse. For advanced users, the Coordinator can also engage in collaborative development, translating high-level methodological suggestions into new, actionable strategies for the lab. The final output of this interaction is a formalized, detailed User Request. This formalized request is then passed to the Gatekeeper, which analyzes the problem formulation and decides the optimal execution path, such as storing data via the storage group or generating new code by routing the task to the SciC, SciML, or both groups. The Gatekeeper is also responsible for managing dependencies, such as first dispatching a task to the SciC group to generate validation data before routing the main PINN task to the SciML group. The Gatekeeper’s final output is a ”modified user request” that serves as the kick-off for the Generative Groups.

Appendix B.2. The Storage Group

The research framework’s knowledge is managed by a specialized Storage Team, which functions as the central curator for all code templates and modules. Its primary role is to pre-process and structure this information to enable a powerful, guided Agentic RAG system. This team consists of two agents: the Analyzer and the Splitter. The Analyzer agent acts as a computational researcher, analyzing all code snippets. For modular, ”cell-based” codes, it labels them and provides a clear description so they can be easily found later. For full PDE solvers, it extracts key metadata, such as the equation and method, into a structured JSON. The Splitter agent then analyzes long code scripts and identifies the most logical line numbers to break them apart for semantic chunking, such as at the end of functions or logical blocks. This knowledge base is dynamic; the user can deposit information directly, and final, validated codes from successful experiments are also fed back to the Storage Team. These agents then analyze and integrate the new solutions, allowing the framework’s knowledge base to grow sequentially over time.

Appendix B.3. The Generative Groups

The generative teams are specialized by domain, including the Scientific Computing (SciC) Group, the SciML PIML Group, and the SciML Operator Learning Group. A key design principle is that all Generative Groups share an essentially identical agentic structure, which allows the framework to apply a consistent, robust process across all problem domains. This shared structure is a complete end-to-end scientific workflow.

Appendix B.3.1. Strategic Team

The evolutionary cycle begins with the Strategy Team, which functions as the ”scientific brain” of the framework. In its autonomous mode, it takes three primary inputs: the modified user request (defining the core problem), the trial history log (detailing all previous experimental runs), and the advisor report. The framework is also designed for expert-in-the-loop collaboration. An advanced user can interact directly with the Strategy Team. In

this mode, the user can enhance, guide, or even directly alter the scientific plan, effectively overriding or supplementing the advisor’s report with their own expertise.

In either operational mode, the advisor report (or the user’s enhanced plan) is the critical driver of the evolutionary loop. It provides the specific scientific diagnosis and the explicit, corrective information (e.g., ”replace the MLP trunk with a KAN trunk”). The Strategist’s primary role is to translate this high-level scientific directive into a concrete, executable plan, while also considering the problem statement and experimental history.

This team utilizes a two-agent ”proposer-critic” configuration. The first Strategist agent (the proposer) synthesizes all inputs—especially the Advisor’s specific cure or the user’s direct interventions—to generate the initial scientific plan. A second Strategist agent (the Critic) then analyzes this plan for logical consistency and potential flaws. For example, it would flag a plan that suggests normalizing inputs from -1 to 1 while simultaneously using a ReLU activation function. This collaborative process ensures the final plan is robust.

This final hypothesis is produced as the scientific strategy report, the master blueprint for the experiment. This report is the core mechanism for evolution, decoupling the Advisor’s high-level scientific curve from the low-level implementation. The scientific strategy report is passed to the Code Retrieval Team. This team is not activated for every cycle; it is specifically engaged when the strategy report calls for new architectures or enhancement modules that are not already part of the active experimental script.

Appendix B.3.2. Code Retrieval Team

The team’s first function, handling the main architecture, involves two key agents: the Retriever and the Validator. The Retriever functions as a specialized RAG system. Its crucial role is to reconstruct long, foundational code templates from a database. This methodology is essential for dealing with a large code database and guarantees that the retrieved reference code does not contain hallucinations. This base code is then passed to the Validator, which performs a critical methodological check. For instance, the Validator ensures the code is appropriate for the problem’s mathematical character, flagging a mismatch such as selecting a global spectral method for a hyperbolic problem.

The team’s second function is to gather the specific enhancement modules. The Collector finds the specific modules and their corresponding submodules (dependencies) from the code library. These are then passed to the Librarian. The Librarian analyzes the full module dataset and, if a required component is missing, is empowered to generate new, complex architectural code from scratch. For example, it could construct a novel Wavelet-KAN architecture. A key aspect of this generation is that the Librarian creates these new components in a modular way, ensuring they are compatible with the main code template.

The Code Retrieval Team’s final outputs—the validated main code template, the required enhancement code (both existing and newly generated), and the scientific strategy report—are then passed to the Implementation Team.

Appendix B.3.3. Implementation Team

This team is a key component of the framework’s first-order operator, receives the scientific strategy report, the base code template, and the enhancement code modules. If the cycle is a re-run due to a crash, it also receives a debug report. The process begins with a ”study phase”. A Planner agent first analyzes the base code and submodules (enhancement

code). It then reads the strategy report (for new features) or the debug report (for bug fixes) to build an internal "mental map" of all required modifications.

Once the specific target cells are identified, a Planner Parser agent translates this analysis into a structured format (e.g., a JSON list of cell indices). This explicit structural step acts as a binding constraint, ensuring that the subsequent modification phase remains strictly focused on the identified components and does not drift into unrelated parts of the codebase.

Following this, the Planner begins a "cell-by-cell refactoring" process using the coordinates provided by the parser. This methodology is crucial for reliably modifying long and complex codebases, as the agent focuses on only one code block, or "cell," at a time. This targeted approach significantly tackles the risk of hallucination. For each targeted cell, the Planner provides a conversational model explanation of the changes, and a Patcher agent immediately transforms this into a structured JSON patch file. This patch specifies the exact lines of code that must be added, deleted, or modified from the main template.

Once the refactoring loop is complete and the code is assembled, the workflow engages an Inspector Agent. This agent acts as a strict verifier, auditing the final executable code against the original Strategy Report. Its role is to ensure that the final implementation faithfully realizes the requested plan without drift or hallucination before passing it to execution.

Appendix B.3.4. Debugging Team

This team handles the complete execution and validation workflow. A Filing Agent within this team runs only on the first iteration of a new experiment. Its sole job is to assign an appropriate, programmatic name for the project directory. After this first run, all subsequent versioning is handled deterministically.

The script is saved in its designated directory and executed. This leads to a fork in the workflow. If the script crashes, the error code and log files are sent to the Debugger agent. The Debugger is in charge of reading the code and the errors, after which it generates a debug report. This report is sent back to the Implementation Team, which will tackle the errors accordingly and generate a new code. This "debug loop" is repeated iteratively until the code is bug-free and runs successfully.

Appendix B.3.5. Advisor Team

If the code runs successfully (i.e., it is bug-free), it proceeds to the Advisor (Review) Team, which is the core of the second-order or meta-reasoning operator for scientific validation. The executed script must generate a comprehensive set of plots, which typically include loss and error convergence, residuals (for PINNs), the reference solution, the prediction, and pointwise errors.

The Advisor agent's analysis is multimodal. It takes the plots, the scientific strategy report, the user question, and the trial history log as its inputs. This diagnostic task is where the Conceptual Scaffolding is critical. The Advisor is aware of and uses these expert blueprints. It maps its qualitative analysis of the plots (e.g., "high error is focalized in one region") to a specific, principled cure derived from the blueprints (e.g., "apply adaptive sampling" per the optimization blueprint). Likewise, by observing the loss curve, it can diagnose issues such as a learning rate that is too high.

This feedback is then processed by the Advisor Parser, a utility agent that translates the Advisor's natural language report into a structured format (like JSON) for easy, machine-

readable processing. This structured output, along with the strategy report, then goes to the Experiment Logging Team. A Register Agent takes this information and updates the trial history log, which serves as the persistent memory for the entire framework. This complete report and updated history are then sent to both the Strategy Team (to inform the next decision) and the user.

By default, the loop is fully automatic. However, the user can intervene at this point to provide high-level suggestions or guide the strategy before the next cycle begins.

Appendix C. User Request Specifications

To ensure reproducibility and transparency regarding the autonomous capabilities of the framework, we provide the exact verbatim “User Requests” (prompts) utilized for the experiments described in Section 3. These requests serve as the initialization input provided to the HENA loop.

Appendix C.1. Numerical Methods

Appendix C.1.1. 2D Inviscid Burgers’ Equation (Exact Solution Discovery)

User Request: Inviscid Burgers

Let’s solve the 2D Inviscid Burgers’ equation:

$$u_t + uu_x + uu_y = 0$$

Domain: $(x, y) \in [0, 4\pi]^2$, $t \in [0, 2]$.

BCs: Periodic in both x and y.

Initial Condition:

$$u(x, y, 0) = \frac{1}{3} + \frac{2}{3} \sin\left(\frac{x+y}{2}\right)$$

The final plot must be saved as `summary_all.png` it should include snapshots of several timesteps.

Appendix C.1.2. Kelvin-Helmholtz Instability (Euler Equations)

User Request: Kelvin-Helmholtz Instability

Let's solve the 2D Compressible Euler equations for the Kelvin-Helmholtz Instability.
Physics Parameters:

- $\gamma = 1.4$
- Viscosity $\mu = 0.0$ (Inviscid flow)
- Gravity $g = 0.0$ (Instability is driven by shear, not buoyancy).

Domain: $(x, y) \in [0, 1.0] \times [0, 1.0]$

Time interval: $t \in [0, 2.5]$

Boundary Conditions:

- x -direction: Periodic
- y -direction: Slip walls (Reflective, normal velocity $v = 0$) at $y = 0$ and $y = 1$.

Initial Conditions: The domain is initialized with a smoothed shear layer at $y = 0.5$.

- Density (ρ): Stratified with a smooth transition.

$$\rho(y) = 1.5 - 0.5 \cdot \tanh\left(\frac{y - 0.5}{0.03}\right)$$

(Density varies from 1.0 at the top to 2.0 at the bottom).

- Pressure (p): Constant uniform pressure. $p = 2.5$
- Velocity:
 - Horizontal (u): Opposing flows smoothed by a tanh profile (Shear layer).

$$u(y) = 0.5 \cdot \tanh\left(\frac{y - 0.5}{0.03}\right)$$

- Vertical (v): A single-mode perturbation to trigger the roll-up.

$$v(x, y) = 0.01 \cdot \sin(4\pi x) \cdot \exp\left(-\frac{(y - 0.5)^2}{0.01}\right)$$

Appendix C.1.3. Rayleigh-Taylor Instability (Navier-Stokes)

User Request: Rayleigh-Taylor Instability

Let's solve the 2D Compressible Navier-Stokes equations for the Rayleigh-Taylor Instability.

Physics Parameters:

- $\gamma = 1.4$
- Viscosity $\mu = 0.001$ (Prandtl number $Pr = 0.72$)
- Gravity $g = 1.0$ acting in the positive y -direction.

Domain: $(x, y) \in [0, 0.25] \times [0, 1.0]$

Time interval: $t \in [0, 3.0]$

Boundary Conditions:

- x -direction: Periodic
- y -direction: No-slip adiabatic walls at $y = 0$ and $y = 1$.

Initial Conditions: The domain is split at $y = 0.5$.

- Density (ρ): A smoothed interface between $\rho_{heavy} = 2.0$ (bottom) and $\rho_{light} = 1.0$ (top).

$$\rho(y) = \rho_{heavy} + (\rho_{light} - \rho_{heavy}) \cdot \frac{1}{2} (1 + \tanh(50(y - 0.5)))$$

- Pressure (p): Hydrostatic balance ($\frac{dp}{dy} = \rho g$).

$$p(y) = \begin{cases} 2y + 1 & \text{if } y < 0.5 \\ y + 1.5 & \text{if } y \geq 0.5 \end{cases}$$

- Velocity: Initialized with zero horizontal velocity ($u = 0$) and a perturbation in vertical velocity (v):

$$v(x, y) = -0.025 \cdot c \cdot \cos(8\pi x) \cdot \sin(\pi y)^6$$

Where $c = \sqrt{\gamma p / \rho}$ is the local speed of sound.

Output: The final plot must be saved as **summary_all.png** and should include snapshots of several timesteps to visualize the mixing.

Appendix C.2. Scientific Machine Learning (PIML)

In these experiments, the reference data used for validation and error metric computation was autonomously generated by the ATHENA Scientific Computing (SciC) group in a prior step and stored in the specific paths indicated in the requests.

Appendix C.2.1. Allen-Cahn Equation

User Request: Allen-Cahn

Let's solve the Allen-Cahn equation:

$$u_t - \epsilon u_{xx} + k(u^3 - u) = 0$$

Physics Parameters: $\epsilon = 0.0001$ and $k = 5$.

Domain: $x \in [-1, 1]$ and $t \in [0, 1]$. Boundary Conditions: Periodic in x .

Initial Condition:

$$u(x, 0) = x^2 \cos(\pi x)$$

Reference Data: You can find the data here: `[path]/allen_cahn.mat`

The solutions are saved as a dictionary with keys 't', 'x' and 'usol'.

Appendix C.2.2. Viscous Burgers' Equation

User Request: Viscous Burgers

Let's solve the Viscous Burgers' equation:

$$u_t + uu_x = \nu u_{xx}$$

Physics Parameters: Viscosity $\nu = 1/(100\pi)$.

Domain: $x \in [-1, 1]$ and $t \in [0, 1]$. Boundary Conditions: Periodic in x .

Initial Condition:

$$u(x, 0) = -\sin(\pi x)$$

Reference Data: You can find the data here: `[path]/burgers.mat`

The solutions are saved as a dictionary with keys 't', 'x' and 'usol'.

Appendix C.2.3. 2D Helmholtz Equation

User Request: 2D Helmholtz

Let's solve the 2D Helmholtz equation:

$$u_{xx} + u_{yy} + k^2 u = g(x, y)$$

Forcing Term:

$$g(x, y) = k^2 u_{an} - (\pi a_1)^2 u_{an} - (\pi a_2)^2 u_{an}$$

Analytical Solution:

$$u_{an} = \sin(\pi a_1 x) \sin(\pi a_2 y)$$

Parameters: $a_1 = 1$, $a_2 = 4$, and $k = 1$.

Domain: $(x, y) \in [-1, 1] \times [-1, 1]$. Boundary Conditions: Periodic in both x and y .

Appendix C.2.4. Korteweg-De Vries (KdV) Equation

User Request: KdV Equation

We are solving a forward problem for the Korteweg-De Vries (KdV) equation:

$$u_t + 6uu_x + u_{xxx} = 0$$

Domain: $t \in [0, 5]$ and $x \in [0, 20]$.

Boundary Conditions:

$$u(0, x) = g_0(x) \quad (ICs)$$

$$u(t, 0) = g_1(t) \quad (BCs1)$$

$$u(t, 20) = g_2(t) \quad (BCs2)$$

$$u_x(t, 20) = g_3(t) \quad (BCs3)$$

The analytical solution is given by the following soliton interaction:

Parameters: $c_1 = 6.0$, $c_2 = 2.0$, $x_1 = -2.0$, $x_2 = 2.0$.

Helper Variables:

$$\zeta_1 = x - c_1 t - x_1$$

$$\zeta_2 = x - c_2 t - x_2$$

Solution Form:

$$u(x, t) = \frac{2(c_1 - c_2) \left[c_1 \cosh^2 \left(\frac{\sqrt{c_2} \zeta_2}{2} \right) + c_2 \sinh^2 \left(\frac{\sqrt{c_1} \zeta_1}{2} \right) \right]}{\left[(\sqrt{c_1} - \sqrt{c_2}) \cosh \left(\frac{\sqrt{c_1} \zeta_1 + \sqrt{c_2} \zeta_2}{2} \right) + (\sqrt{c_1} + \sqrt{c_2}) \cosh \left(\frac{\sqrt{c_1} \zeta_1 - \sqrt{c_2} \zeta_2}{2} \right) \right]^2}$$

Appendix C.2.5. 1D Inviscid Burgers' Equation (Shock Formation)

User Request: Inviscid Burgers (PIML Stress Test)

Let's solve the 1D Inviscid Burgers' equation:

$$u_t + uu_x = 0$$

Domain: $x \in [-1, 1]$ and $t \in [0, 1]$. Boundary Conditions: Periodic in x .

Initial Condition:

$$u(x, 0) = -\sin(\pi x)$$

Reference Data to compute error metrics: `[path]/burgers.npz`

The code that generated the data saves `burgers.npz` in NPZ format containing keys: 't' (200,), 'x' (256,), 'usol' (200x256).

Appendix C.3. Operator Learning (DeepONet)

User Request: Viscous Burgers

Let's solve the Viscous Burgers' equation:

$$u_t + uu_x = \nu u_{xx}$$

Domain: $x \in [0, 1]$ and $t \in [0, 1]$.

Boundary Conditions: Periodic in x .

Physics Parameters: Viscosity $\nu = 1/1000$ (High Reynolds number regime).

Problem Definition: This task requires building an Operator Network that learns the mapping from the initial condition $u(x, 0)$ to the full spatio-temporal solution $u(x, t)$ up to t_{end} (where t_{end} should be extracted directly from the reference data).

Reference Data:

You can find the training data here:

`[path]/Burger_1000_5000.mat`

Appendix C.4. Artificial Intelligence Velocimetry (Hybrid Workflow)

In this closed-loop experiment, the system must perform a forward numerical verification using parameters inferred from a previous inverse step.

Appendix C.4.1. Step 2: Inverse Problem (Reynolds Number Inference)

User Request: Inverse Navier-Stokes (Re Inference)

Let's solve an inverse problem for the 2D steady-state incompressible Navier-Stokes equations (lid-driven cavity):

$$\begin{aligned}\nabla \cdot \mathbf{u} &= 0 \\ (\mathbf{u} \cdot \nabla) \mathbf{u} &= -\nabla p + \frac{1}{Re} \nabla^2 \mathbf{u}\end{aligned}$$

Domain: $(x, y) \in [0, 1] \times [0, 1]$

Boundary Conditions:

- Top wall ($y = 1$): $\mathbf{u} = (1, 0)$ (moving lid)
- Bottom wall ($y = 0$): $\mathbf{u} = (0, 0)$ (no-slip)
- Left wall ($x = 0$): $\mathbf{u} = (0, 0)$ (no-slip)
- Right wall ($x = 1$): $\mathbf{u} = (0, 0)$ (no-slip)

Task: Find the Reynolds number (Re) by solving an inverse problem.

Training Data: Randomly sample 100 points from the interior of the domain (excluding boundaries) from the reference dataset. Use only the velocity components (u, v) at these sampled points for training. Do NOT use pressure data for training.

Reference Data (for computing error metrics only): Path: `[path]/ldc.npz`

The reference dataset is unstructured and is an NPZ format containing keys: 'x', 'y', 'u', 'v', 'p', 'Re'.

- 'x', 'y': Node coordinates (1D arrays)
- 'u', 'v': Velocity components at each node
- 'p': Pressure at each node

The true $Re = 500$. Use it only for computing error metrics.

Evaluation: After training, compute error metrics using the FULL reference dataset (all points, including u, v , and p). Report the predicted Reynolds number and compare it to the true value from the reference data.

Saving data: Please save the data as an npz file including the learned 'Re' number, and the sensor points coordinates and values 'x_sensor', 'y_sensor', 'u_sensor' and 'v_sensor'.

Appendix C.4.2. Step 3: Numerical Verification (Forward Solver)

User Request: Lid-Driven Cavity (Forward Verification with Inferred Re)

Let's solve the inverse 2D steady-state incompressible Navier-Stokes equations (lid-driven cavity):

$$\begin{aligned}\nabla \cdot \mathbf{u} &= 0 \\ (\mathbf{u} \cdot \nabla) \mathbf{u} &= -\nabla p + \frac{1}{Re} \nabla^2 \mathbf{u}\end{aligned}$$

Domain: $(x, y) \in [0, 1] \times [0, 1]$; Here $Re = 525$.

Boundary Conditions:

- Top wall ($y = 1$):

$$u(x, 1) = 1 - \frac{\cosh(C_0(x - 0.5))}{\cosh(0.5C_0)}$$

where the constant is set to $C_0 = 50$.

- Bottom wall ($y = 0$): $\mathbf{u} = (0, 0)$ (no-slip)
- Left wall ($x = 0$): $\mathbf{u} = (0, 0)$ (no-slip)
- Right wall ($x = 1$): $\mathbf{u} = (0, 0)$ (no-slip)

Cross Validation:

— Sensors: The data was saved as: Path: `[path]/results.npz`

Details: Saves 'results.npz' containing keys: 'x_sensor', 'y_sensor', 'u_sensor', 'v_hidden_at_sensor', 'Re_est', etc.

This file contains a list of sensors. Once the numerical solution is obtained, please evaluate it on the sensor points and report the relative L2 error of u and relative L2 error of v.

— True Data: Path: `[path]/ldc_Re500.npz`

The dataset is unstructured and was saved as an NPZ format containing keys: 'x', 'y', 'u', 'v', 'p'

- 'x', 'y': Node coordinates (1D arrays)
- 'u', 'v': Velocity components at each node
- 'p': Pressure at each node

The true solution is here; please report the L2 error for u and v of the true solution against the new numerical solution.

Output: The final plot must be saved as `summary_all.png`.